Chapter 5: Experimental modelling of seismic pile-soil interaction in level ground

5.1 Introduction

Each of the centrifuge tests carried out generated data equivalent to a real earthquake that can be viewed from different angles, such as study of pile behaviour or pore pressure generation and dissipation in the soil, etc. This thesis mainly deals with the data pertaining to the scope of the research work mentioned in section 1.8. However, the raw data from the tests can be found in Appendix-D. This chapter mainly presents the relevant results of the centrifuge tests to verify the proposed hypothesis of pile failure (section 3.5). Detailed discussion of the test results in relation to the verification of the proposed hypothesis and pile-soil interaction can be found in chapter 6.

As mentioned in Tables 4.3 and 4.12, a series of five centrifuge tests with model (Dural) piles have been carried out to verify the proposed hypothesis of pile failure and show pile-soil interactions during seismic liquefaction. The first three tests SB-02, SB-03 and SB-04 were aimed at verifying the hypothesis of pile failure by buckling instability, the results of which are presented in sections 5.2 and 5.3. In these tests the different load effects were decoupled as described in section 4.10.1. Test SB-04 was repeated as SB-05 with no soil. This test was carried out to distinguish the behaviour of model pile in the absence of soil, the results of which are presented in section 5.3. Test SB-06 was dedicated to understanding some more detailed aspects of pile-soil interaction during seismic liquefaction.

The instrumentation layouts for each test along with a photograph of the centrifuge package can be seen in Figures 5.1(a&b) through 5.5(a&b). Each set of figures is placed on the same page to

compare the schematic diagram of the experiment with the physical model. Details of placing the instruments and their working principles are discussed in chapter 4. In the figures, pile head masses are quoted. From Figure 5.1(a) it must be noted that in test SB-02, there was a layer of rock flour (silt) at the top of the liquefiable soil, which was intended to hold the excess pore pressure for longer duration. In Figure 5.3a (test SB-04) for the pile having 1.78kg pile head mass and in Figure 5.5a (test SB-06) for the pile having 1.5kg pile head mass, PPT's were placed in the direction of permitted buckling i.e. transversely to the direction of shaking. Table 5.1 summarises the information about the earthquake motions imparted in the tests.

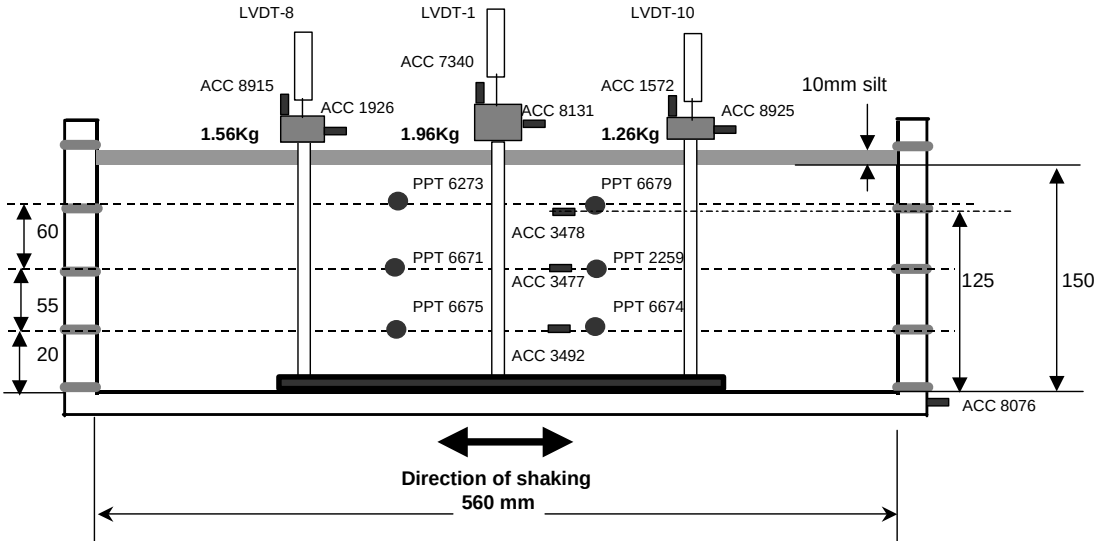

Figure 5.1(a): Model layout and instrumentation in test SB-02 (All dimensions are in mm).

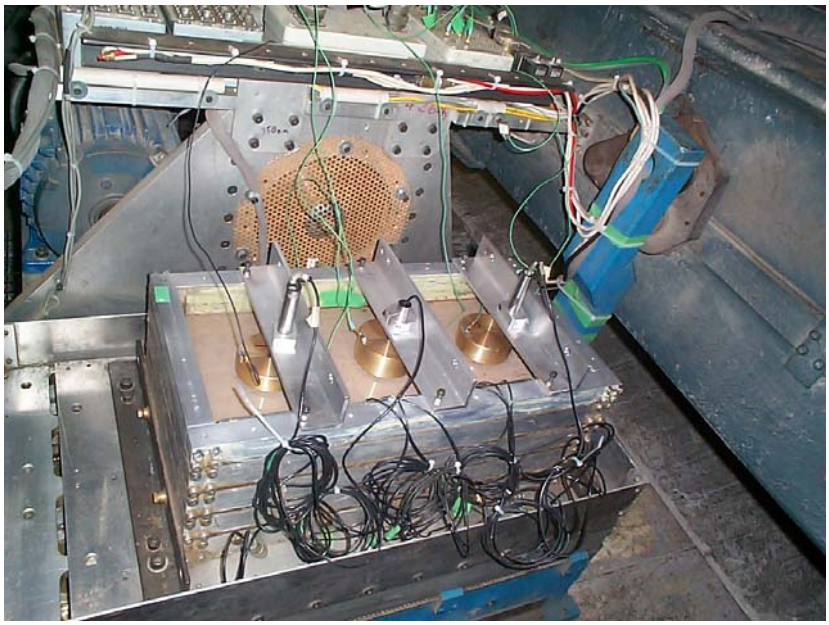

Figure 5.1(b): Package SB-02 before the test.

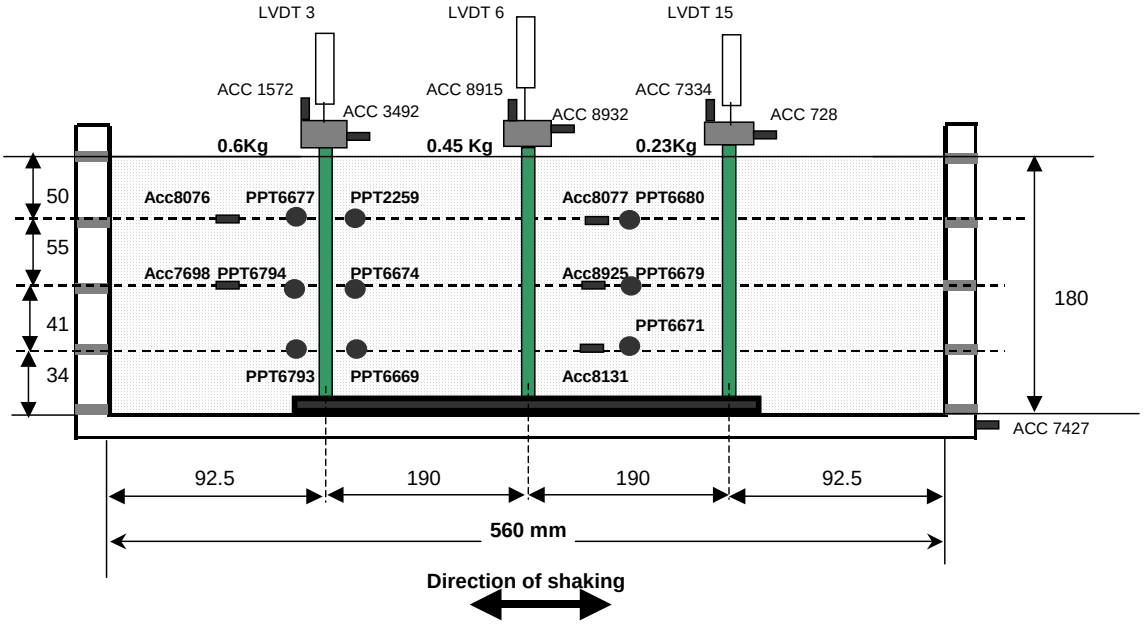

Figure 5.2(a): Model layout and instrumentation in test SB-03 (All dimensions are in mm).

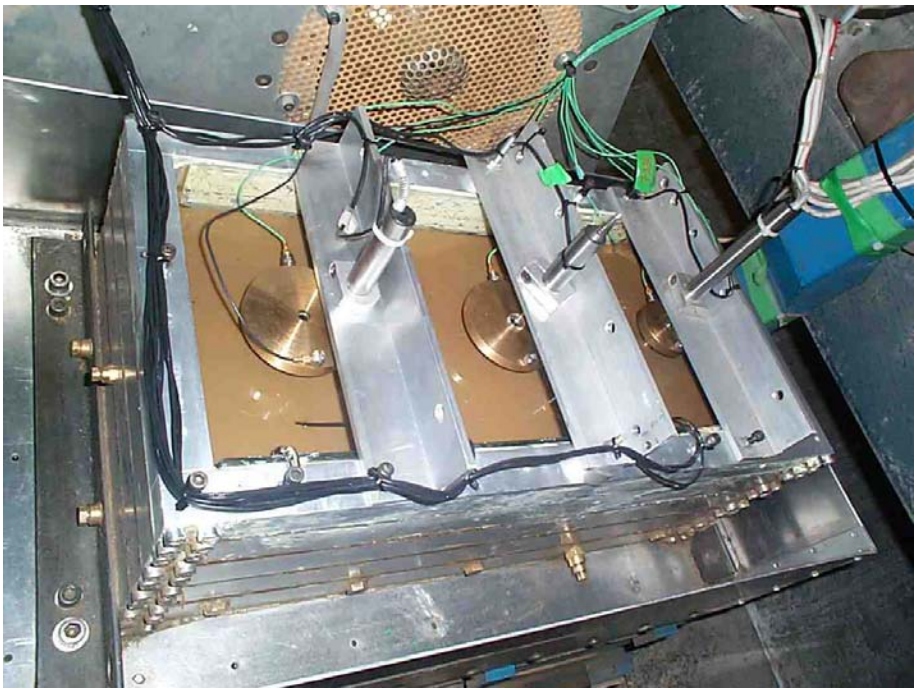

Figure 5.2(b): Package SB-03 before the test.

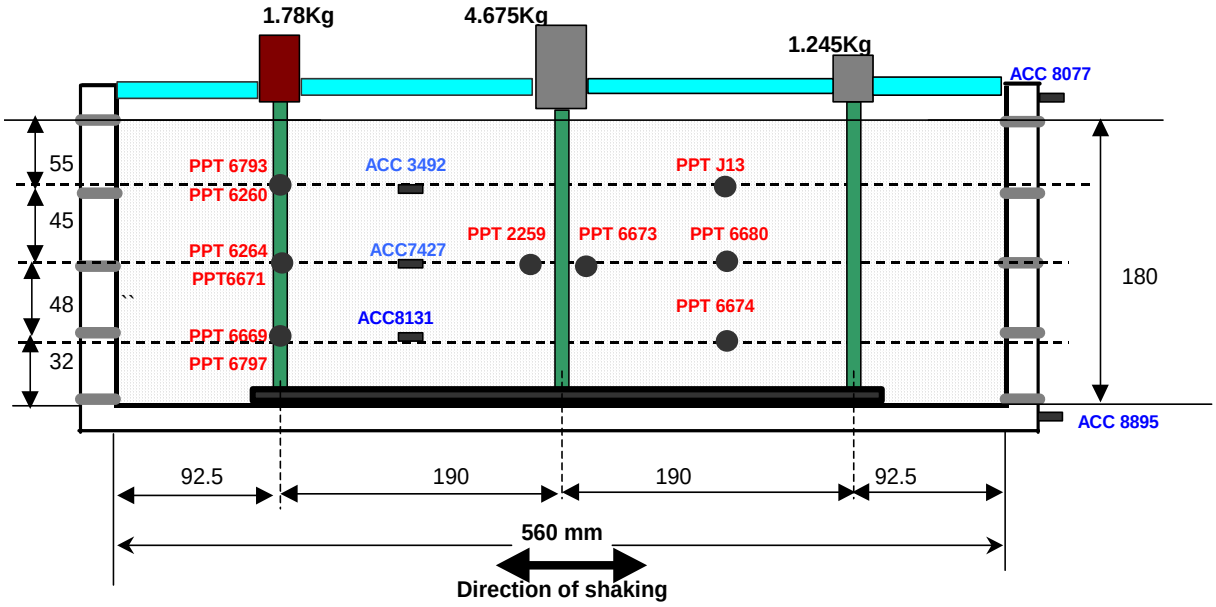

Figure 5.3(a): Model layout and instrumentation layout in test SB-04. Details of instruments layout for the pile having head mass of 1.78kg can be found in Figure 5.17. (All dimensions are in mm).

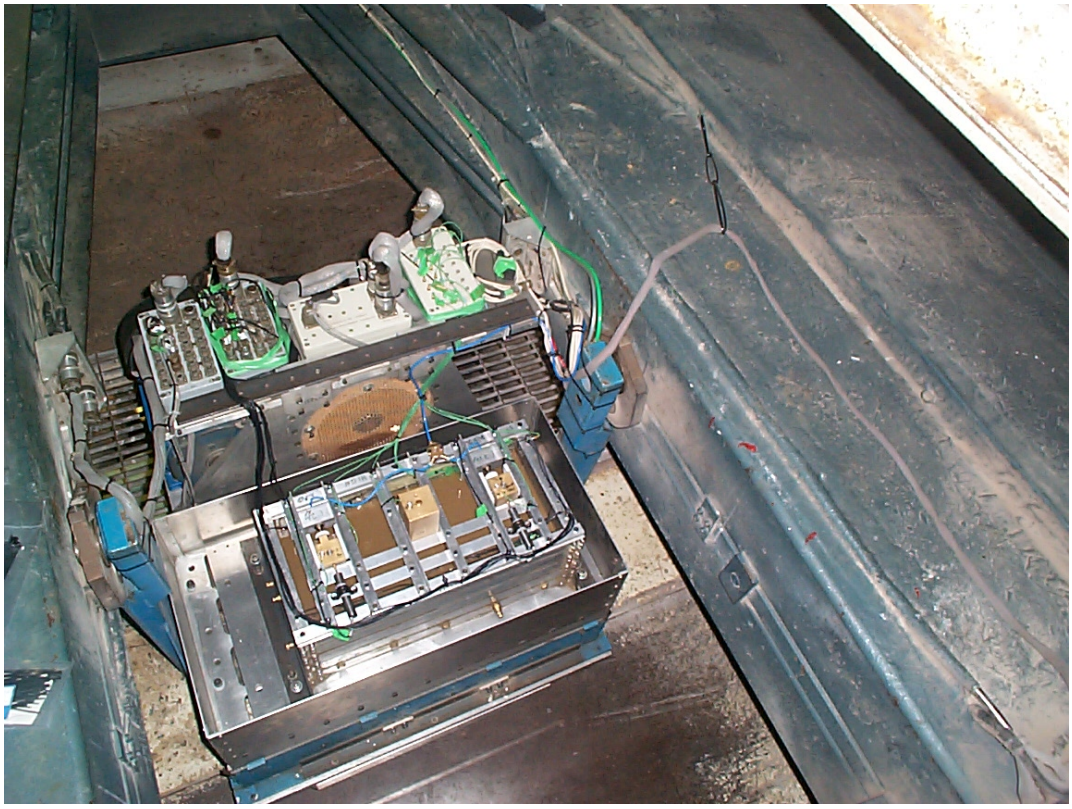

Figure 5.3(b): Package SB-04 before the test. A closer view is shown in Figure 4.29

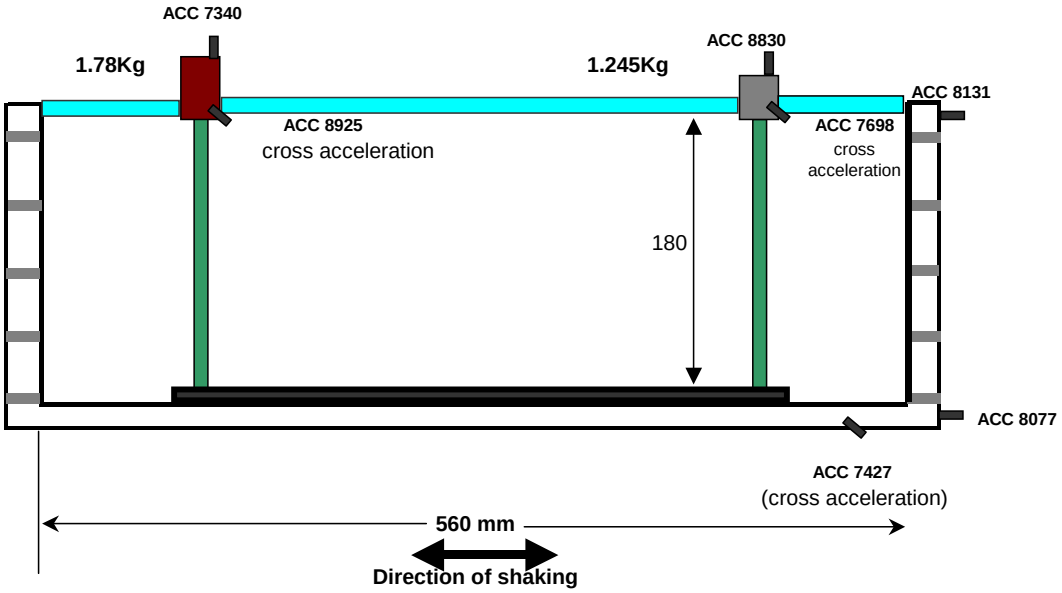

Figure 5.4(a): Model layout and instrumentation in test SB-05 (All dimensions are in mm).

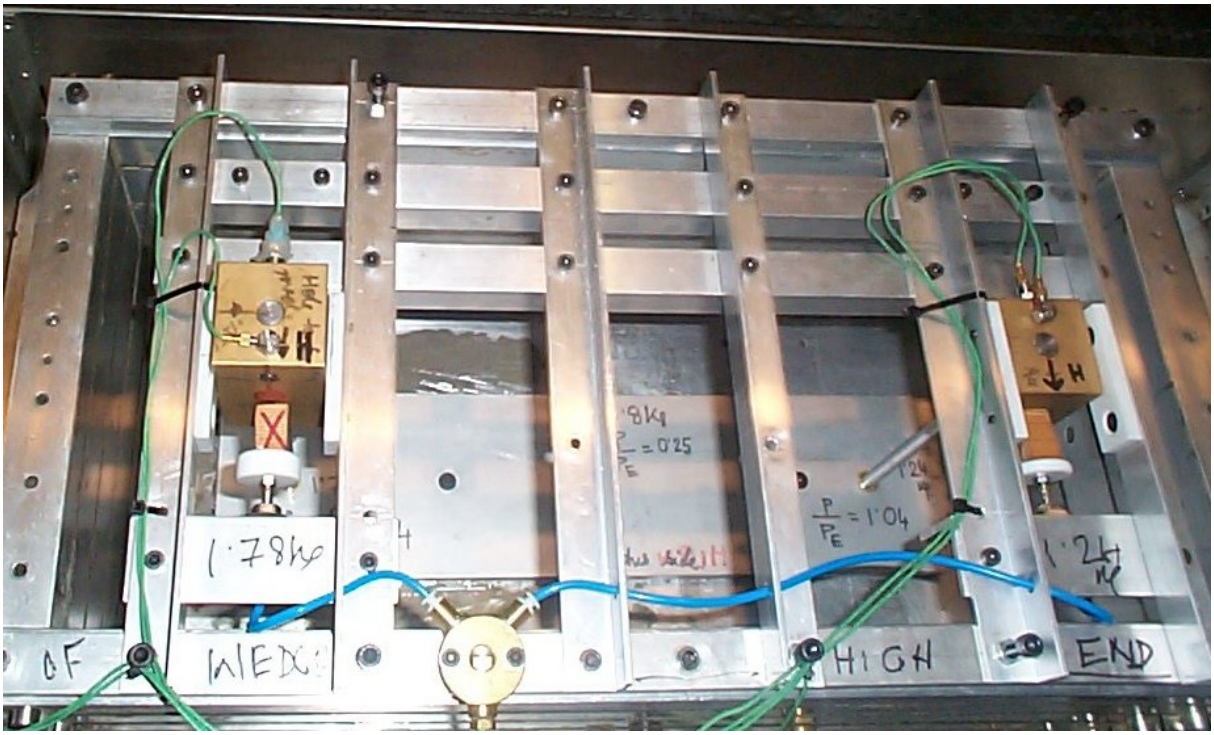

Figure 5.4(b): Package SB-05 before the test

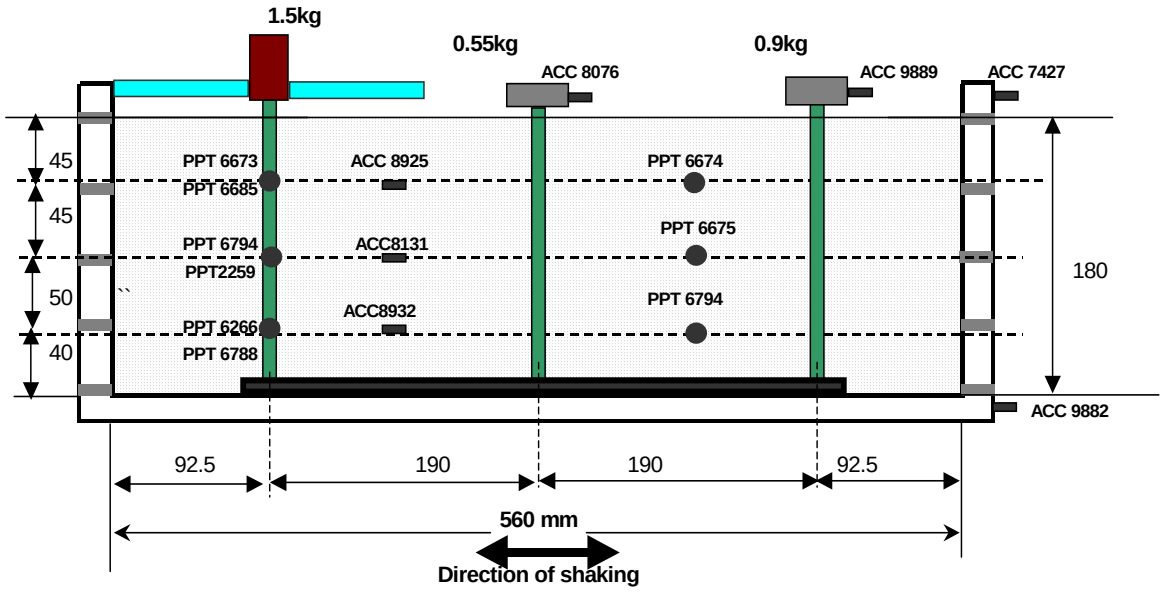

Figure 5.5(a): Model layout and instrumentation in test SB-06. Some instruments are not shown here for clarity. Detailed instrumentation for the pile having head mass of 1.5kg can be seen in Figure 5.20. (All dimensions are in mm).

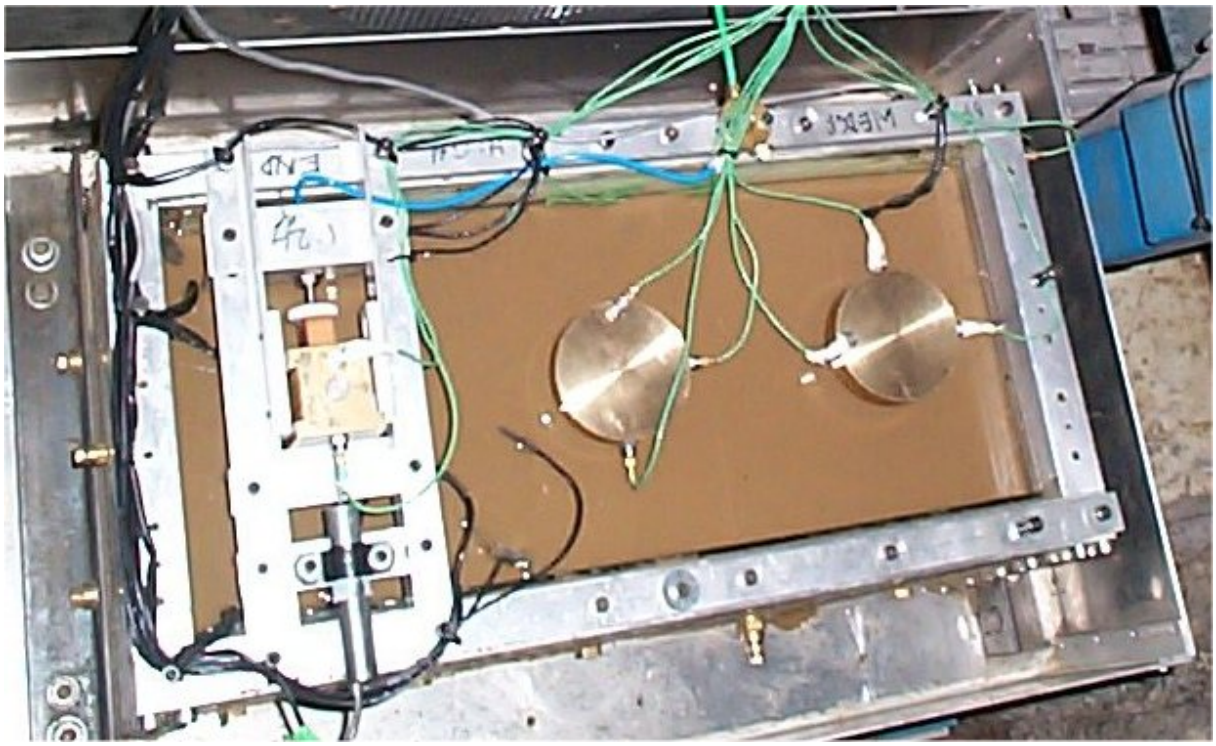

Figure 5.5(b): Package SB-06 before the test

Table 5.1: Earthquakes fired in the tests

Test ID	Earthquake (model scale)			Remarks
	Magnitude PGA	Duration	Frequency	
SB-02	8.7g (17.4%)	0.5s	50Hz	One earthquake fired
SB-03	5.69g (11.38%) 5.84g (11.68%) 5.69g (10.54%) 7.3g (14.6%)	0.5s 0.5s 0.9s 0.9s	50Hz	4 earthquakes were fired None of the piles failed
SB-04	6.77g(13.54%)	0.9s	50Hz	One earthquake fired
SB-05	7.77g (15.54%)	0.5s	50Hz	One earthquake fired
SB-06	8.5g (17%) 6g (12%)	0.9 s 2.5s	50Hz	The second earthquake was due to actuator problem

5.1.1 Visual observation after the tests

It is quite well known that the most recognised field evidence of soil liquefaction is the presence of sand boils at the ground surface following an earthquake, as shown in Figures 5.6 (a&b). Also if the upward hydraulic gradient is high enough sand particles from below can be carried to the ground surface. Figures 5.7 through 5.11 shows the visual observations after the tests. Observations similar to Figures 5.6 (a&b) have been noticed after the test SB-02, Figure 5.7 (silt was only present in test SB-02). Sand boils can be seen at the surface and sand particles erupted from below piercing the top silt layer. This demonstrates that liquefaction occurred in the centrifuge model.

Figures 5.7, 5.9 and 5.11 show the surface observation of the piles after the tests. It must be noted that the piles that failed had their heads rotated which is quite similar to the visual observations of the piled structures after an earthquake (see Figures 1.2(c)). This demonstrates that centrifuge modelling can reproduce physical mechanisms observed at real earthquakes. It must also be noted that the model piles in the experiments were in level ground whereas the collapsed piled structures were in laterally spreading soil. A detailed discussion on replication of the mechanism can be found in section 6.3.

Figure 5.6: Sand boils, (a) after the 1999 Chi-Chi earthquake (Taiwan); (b) after the 2001 Bhuj earthquake (India).

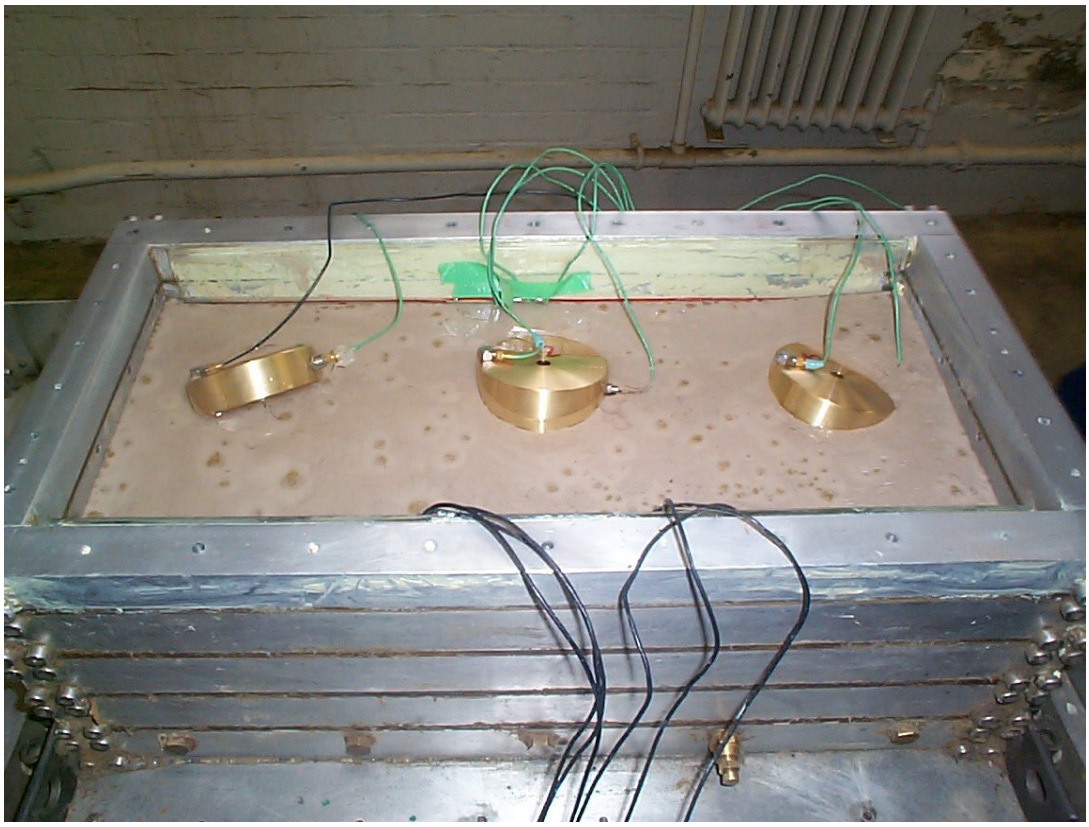

Figure 5.7: Surface observation after the test SB-02.

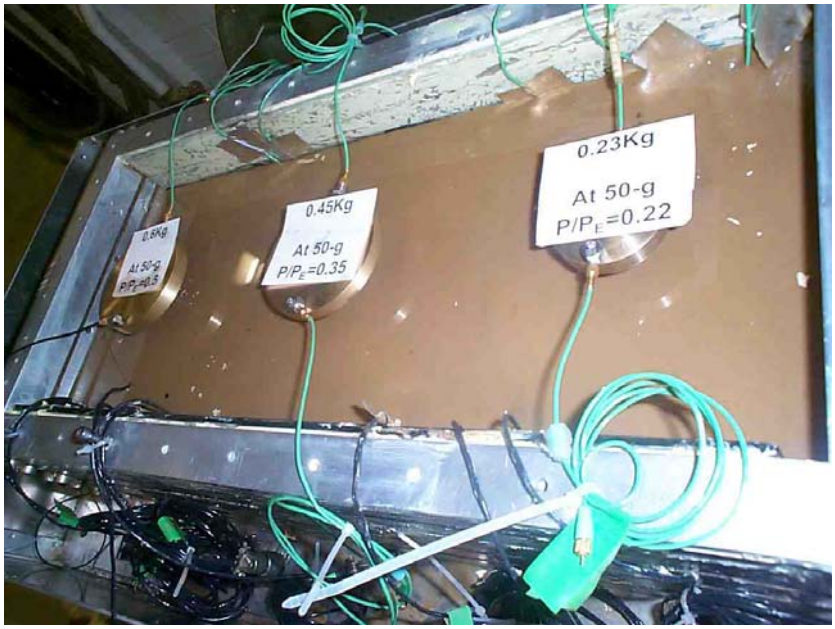

Figure 5.8: Surface observation after the test SB-03

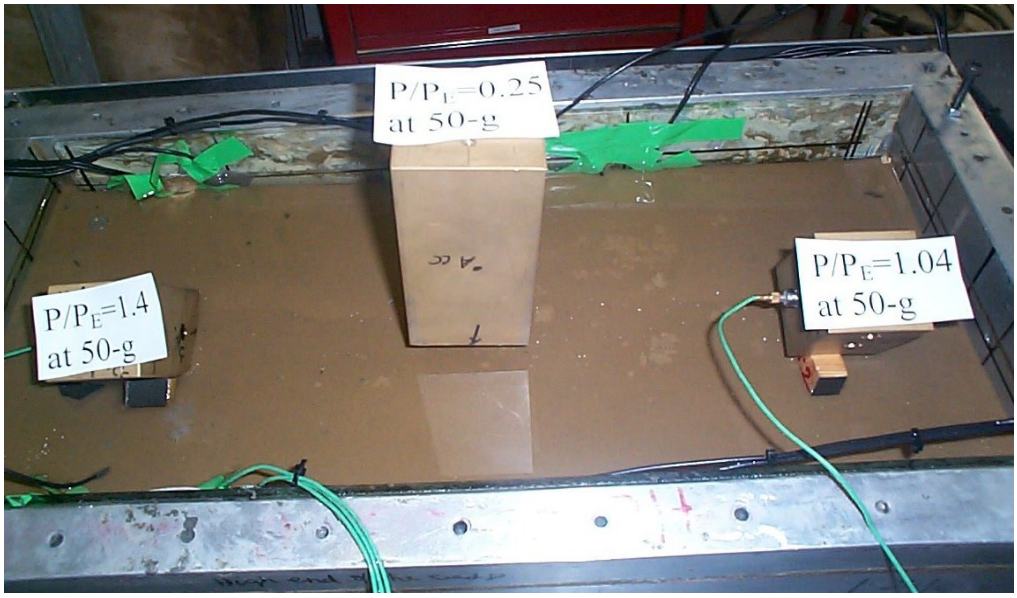

Figure 5.9: Surface observation after the test SB-04.

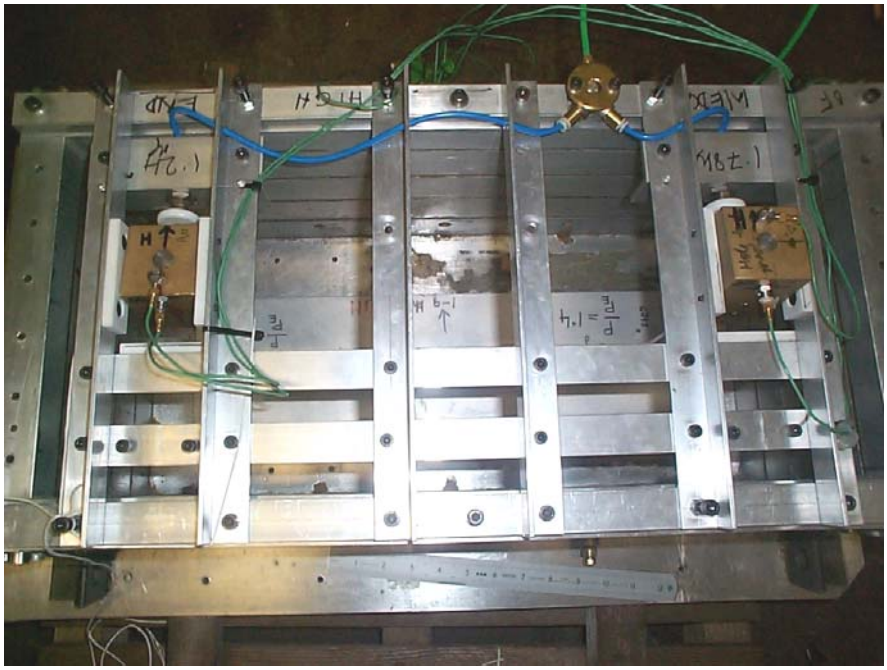

Figure 5.10: Surface observation after the test SB-05

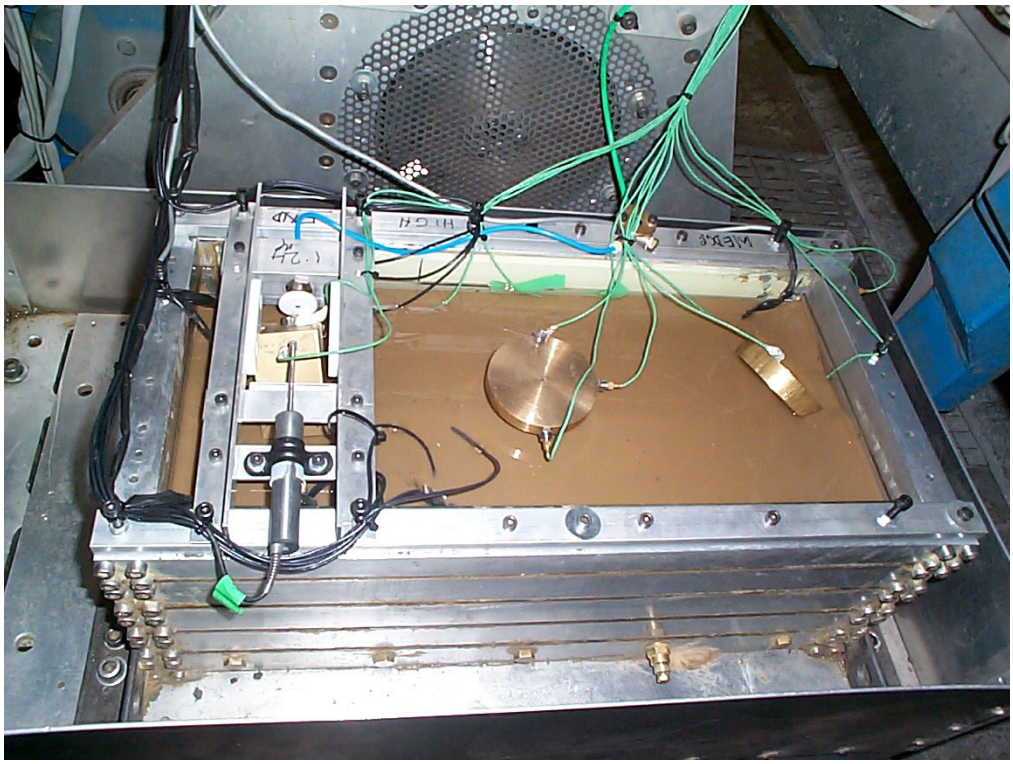

Figure 5.11: Surface observation after the test SB-06.

5.2 Summary of pile performances and verification of the hypothesis

Figure 5.12 shows the schematic representation of the five tests emphasising the normalised axial load (P/P_{cr}). In the figure, P denotes the applied axial load on the pile and P_{cr} represents the elastic critical load of the pile treated as a column neglecting any support from the soil. It can be observed that piles having P/P_{cr} ratio less than 0.5 did not fail even after a series of earthquakes, (see test SB-03 in Table 5.1). On the other hand piles having P/P_{cr} ratio greater than 0.75 failed during an earthquake either under the action of axial load or combined axial load and inertia. This result is consistent with the study of case histories where the piles that failed had P/P_{cr} ratio between 0.5 and 1.0 (see Figure 3.26).

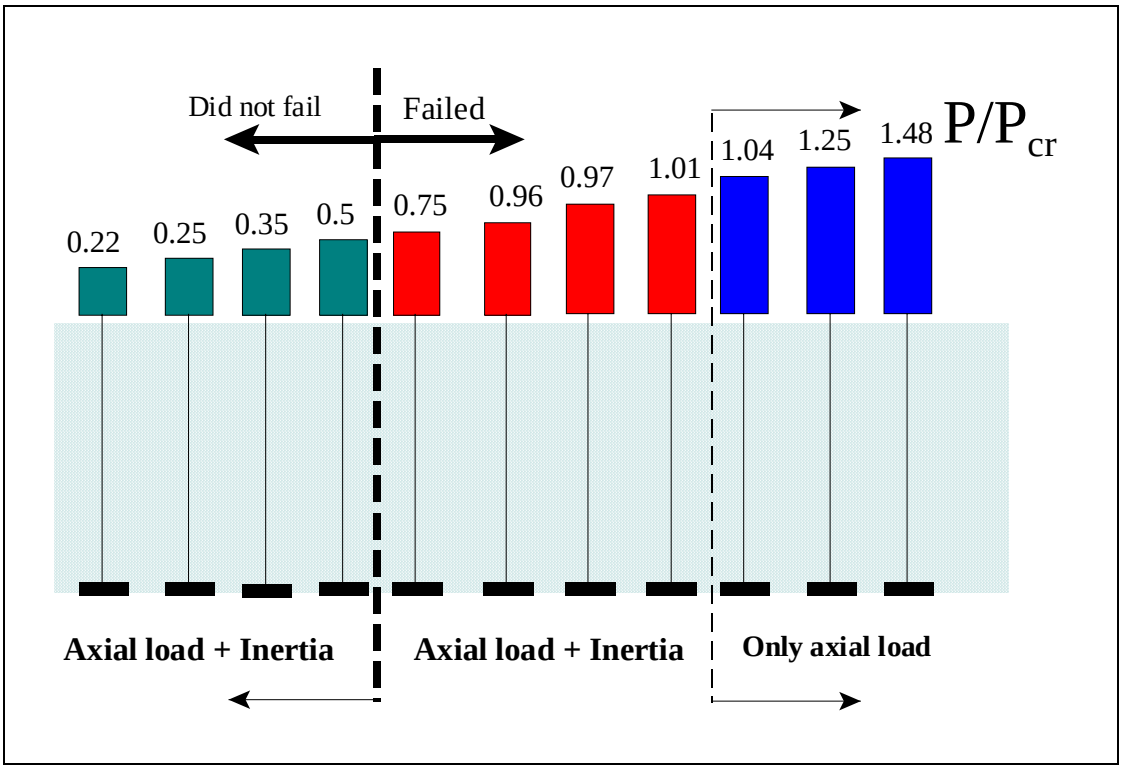

Figure 5.12: Schematic representation of the test results.

The summary of the performance of the 12 piles in tests SB-02, SB-03, SB-04 and SB-06 is shown in Table 5.2. The test results of SB-05 are not included in the table, as the test was identical to SB-04 except that it did not have soil, and so the model piles act as cantilever struts. It can be seen that in tests SB-02, SB-04 and SB-06 all piles (expect pile 12) which should have failed, did fail, whereas the piles in SB-03 and SB-06 that should not have failed according to the buckling criterion, did not fail.

Pile failure in SB-02 cannot be positively attributed to the effects of axial load since lateral loads were also applied, whereas in test SB-04 the load was purely axial at failure. It can be concluded that tests SB-03 and SB-04 support the hypothesis of pile failure occurring for $P/P_{cr} \geq 1$.

Figure 5.13 shows the slenderness ratio of the pile plotted against the mean axial stress. In the figure the yield stress line, Euler's elastic instability curve and Rankine's combined buckling curve are plotted. The graph has a close resemblance with the observed case histories of pile foundation performance during past earthquakes, as shown in Figure 3.25.

Table 5.2: Performance of the piles during the centrifuge tests

Test ID	**Pile ID**	**Head mass** kg	**Max load P** N	**P/A** MPa	**L_{eff} (L_{eff}/r_{min})**	**P/P_{cr}**	**Remarks**
SB-02 Pile length = 160mm r_{min} =3.1mm A=9.7 mm²	1	1.96	768	79	L_{eff} = 355mm 114	0.97	Failed at 40-g during swing up
	2	1.56	642	65	L_{eff} = 350mm 113	1.01	Failed at 42-g during swing up
	3	1.26	617	63	L_{eff} = 345mm 111	0.97	Failed during earthquake
SB-03 Pile length = 180mm r_{min} =3.1mm A = 11.2 mm²	4	0.60	294	26.3	L_{eff} = 372mm 120	0.5	Did not collapse
	5	0.45	220	19.7	L_{eff} = 370mm 119	0.35	Did not collapse
	6	0.23	113	10.1	L_{ef} = 370mm 119	0.22	Did not collapse
SB-04 Pile length = 180mm r_{min} = 3.1mm A = 11.2 mm²	7	1.25	610	54.5	L_{eff} = 420mm 135	1.04	Failed during earthquake
	8	1.78	872	78	L_{eff} = 445mm 144	1.48	Failed during earthquake
	9	4.68	2249	201	L_{eff} = 90mm 29	0.25	Did not collapse
SB-06 Pile length = 180mm r_{min} = 3.1mm A = 11.2 mm²	10	1.5	735	65.6	L_{eff} = 445mm 144	1.25	Failed during earthquake
	11	0.55	269	24	L_{eff} = 370mm 119	0.46	Did not collapse
	12	0.9	441	39.4	L_{eff} = 378mm 122	0.75	Failed during earthquake

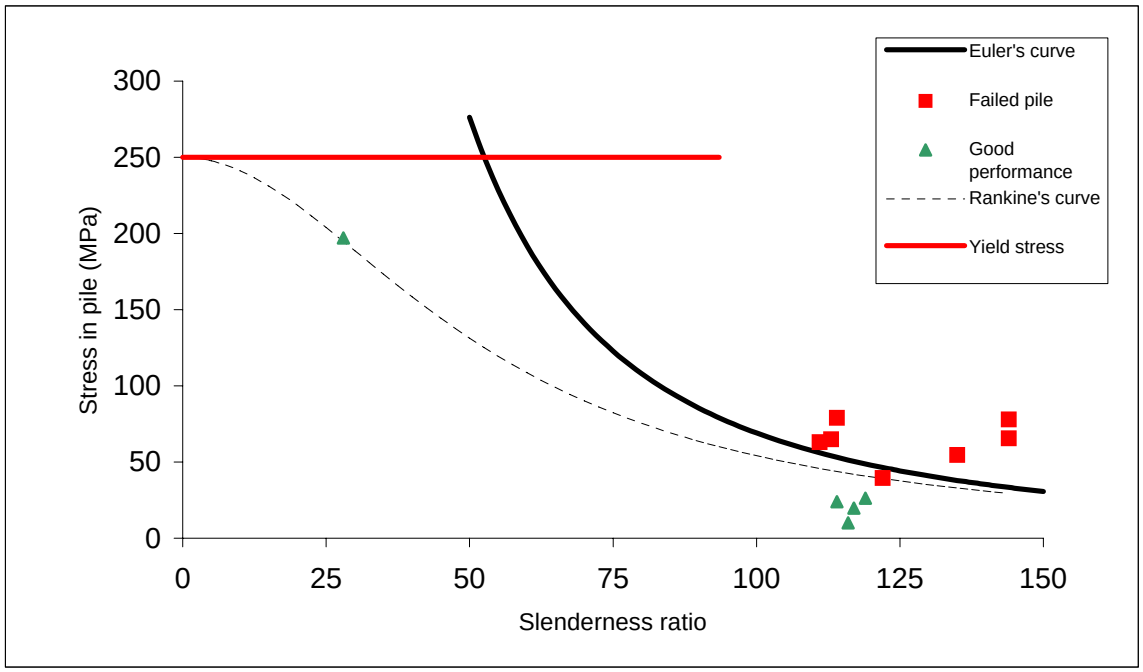

Figure 5.13: Performance of the piles after the tests.

In the analysis of the centrifuge test results presented in this thesis, the length of the pile is assumed to be the distance between the C.G of the pile head mass (brass block) and the point of fixity at the bottom of the ESB box. The pile being sufficiently long compared to the dimension of the pile head mass, the correction due to the stiffening effect of the block in the upper part of the pile will be negligible and was ignored in the analysis.

5.3 Behaviour of pile under axial load alone

One of the aims of this research is to improve understanding of the effects of axial load on a pile during soil liquefaction and hence experiments SB-04 and SB-05 were carried out. This section of the chapter presents the results of these tests. It must be remembered that one-dimensional shaking was imparted in the model, the pile head was restrained in the direction of shaking and hence, the test results are due to the effects of axial load alone. Figure 5.14 (a) shows pile 7 partially revealed after the testing during excavation and Figure 5.14 (b) shows the pile after the excavation was complete. In test SB-05, an identical pile was tested in the absence of soil and Figure 5.14 (c) shows that pile after the test. Similar forms of buckling has been observed as shown in Figure 5.15 for pile 8, and thus we can conclude that this observation is repeatable.

In both tests, the piles buckled in the transverse direction, i.e. orthogonal to the direction of shaking. In test SB-04 the hinge formed about one third the way down the liquefiable soil whereas in test SB-05 the hinge formed at the bottom third of the pile in air.

The only force other than axial force acting in the direction of pile movement is the imperfection force in the pile head mass due to cross acceleration of the SAM actuator. This force was measured to be 5% of the main acceleration i.e. 2.45m/sec^2 corresponding to a 0.1% earthquake component. For pile 8 the head mass is 1.78 kg and hence the unwanted lateral force is 1.78 kg × 2.45m/sec^2 = 4.3N and this is clearly unable to cause a bending failure in pile in which a hinge formed at 40mm below the pile head. The only possible explanation for the pile failure in SB-04 is buckling instability of pile. This demonstrates that if the axial load in a pile is high enough it can cause failure to the pile during liquefaction.

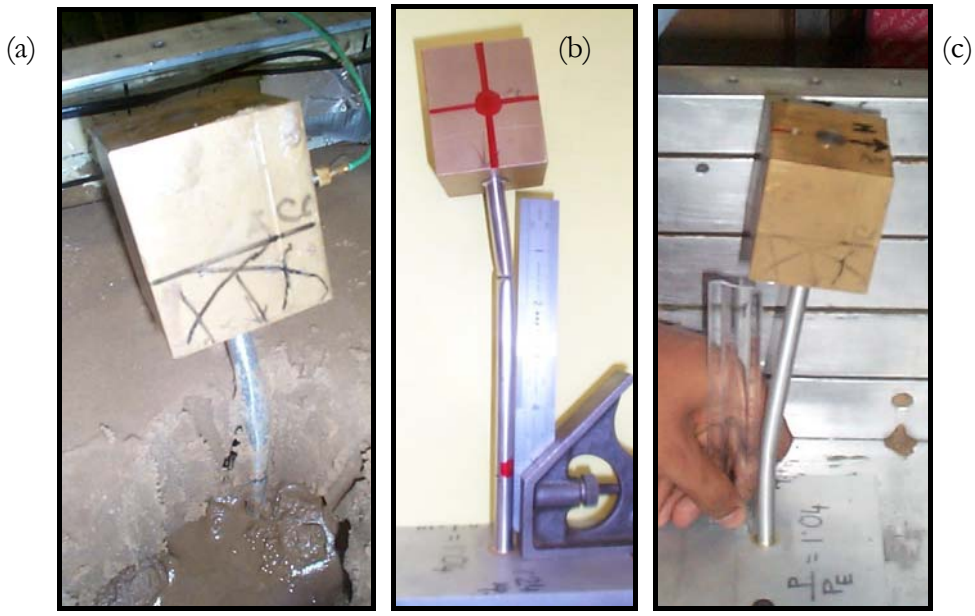

Figure5.14: (a) Mode of failure of pile 7 in test SB-04 during excavation; (b): Pile 7 after excavation in test SB-04; (c): Same pile in test SB-05.

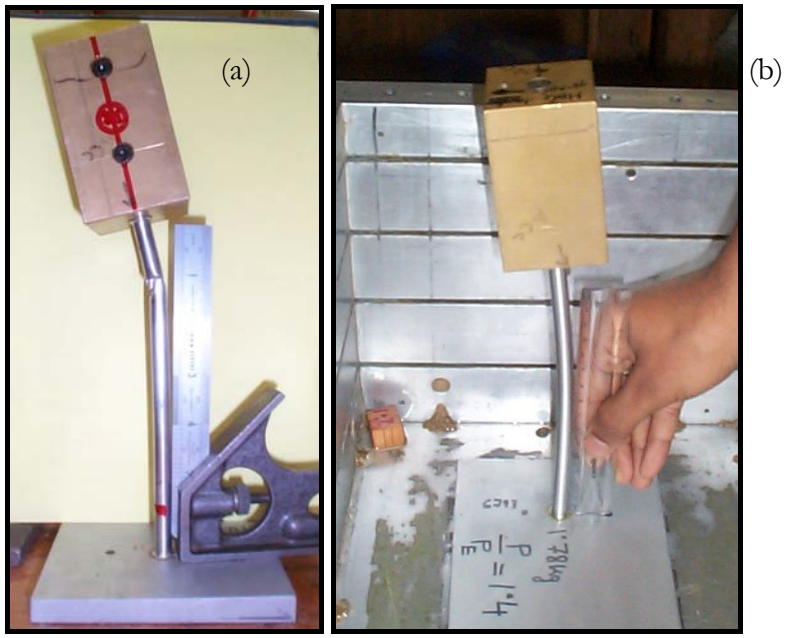

Figure 5.15: (a): Mode of failure of pile 8 in test SB-04; (b): Mode of failure of the same pile in test SB-05.

Figure 5.16 shows schematically the mode shapes of the buckled pile in the two tests. It is interesting to note the difference in mode shapes of the buckled pile in the two tests. Curvature being related to bending moments, the reduction of curvature below the plastic hinge in SB-04 demonstrates the existence of lateral resistance from the soil. Section 6.5 discusses more on the formation of shallow hinge formation in the case of pile buckling.

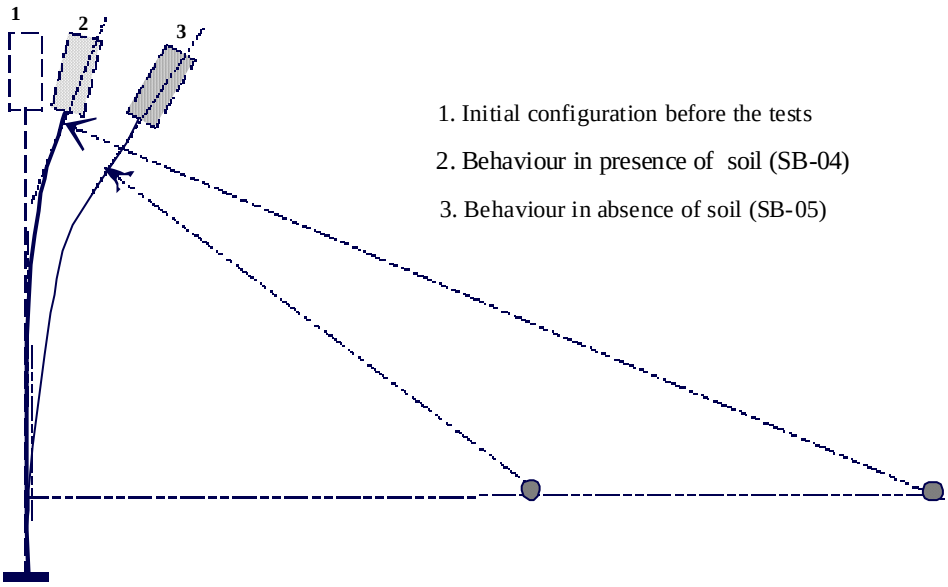

Figure 5.16: Comparison of the buckling mode shape of pile in tests SB-04 and SB-05

5.3.1 Excess pore pressure generation

Figure 5.17 shows the instrumentation layout with pore pressure transducer locations surrounding pile 8 (test SB-04, Table 5.2) and also in the free field. Figure 5.18 shows the free field traces of excess pore pressure. It may be noted that as the shaking starts the pore pressure rises in the soil starting from the top and proceeding downwards. In every case, at a time of about 0.5 seconds in the history, or about 0.25s after shaking started, the excess pore pressures δu in the free field reach a plateau. Figure 5.18 shows that in each case the plateau corresponds well with an estimate of the pre-existing effective vertical stress at the corresponding elevation, suggesting that σ'_v had fallen to zero. Between 0.5s and 1.0s in Figure 5.18, the pile will have lost all lateral effective stress in a progressive fashion, top-down. This is observed in all the centrifuge tests.

It must also be observed from the pore pressure traces that the upper part of the liquefiable sand layer remains longest in a state of "zero effective stress". Figure 5.19 shows the isochrones at an interval of 1 sec in test SB-02. In the figure "Hy st" represents the line of hydrostatic pressure and "liq l" represents the line of zero effective stress. It can be seen that dissipation occurs bottom up which again substantiates the fact that the upper part of the liquefiable layer remains

in a state of zero effective stress for a longer duration due to upward hydraulic gradients (see Brennan, 2003).

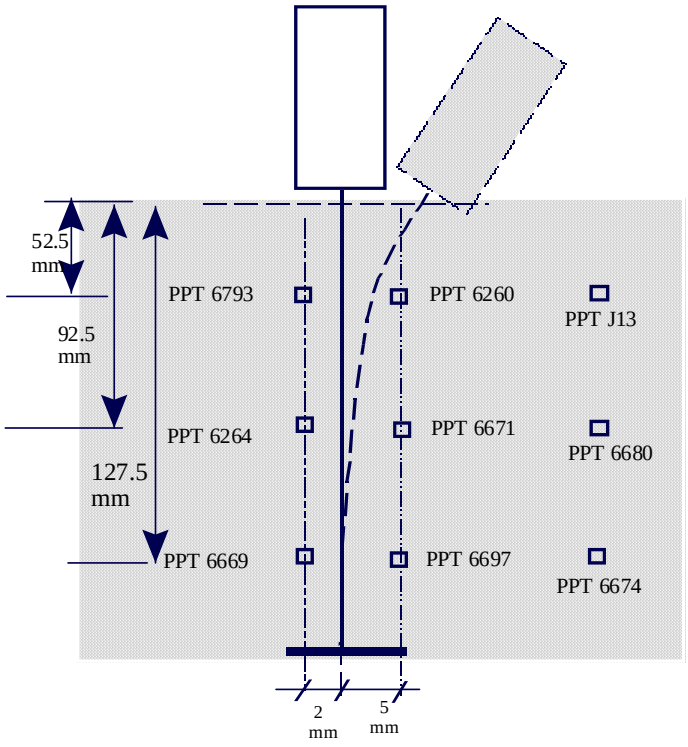

Figure 5.17: Instrumentation layout surrounding Pile 8.

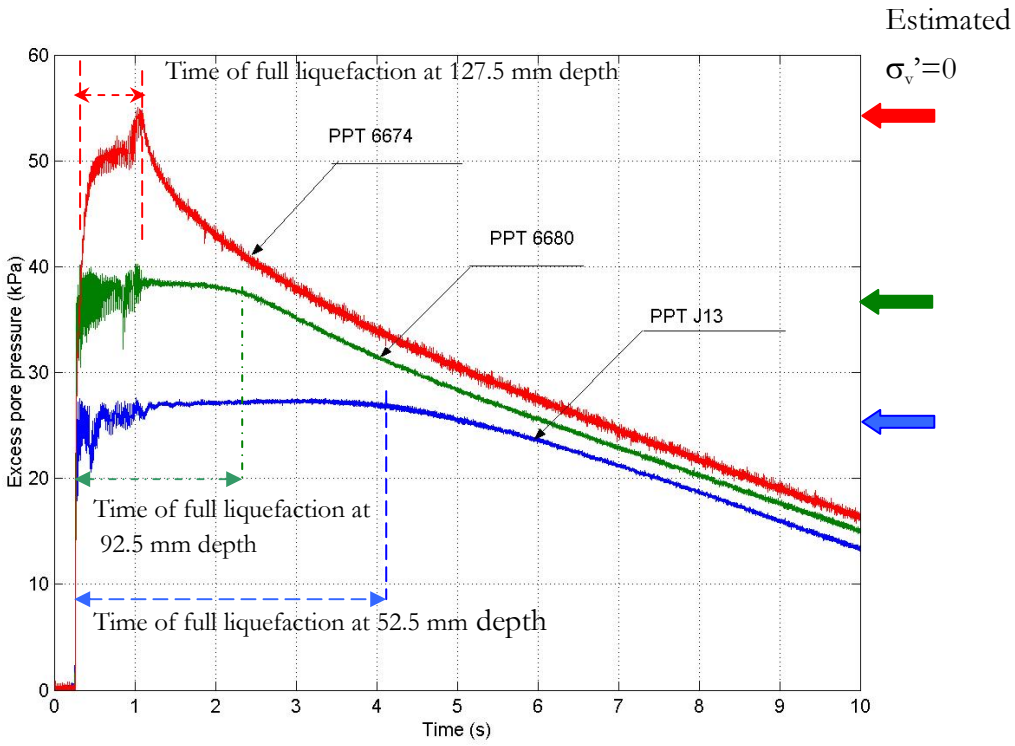

Figure 5.18: Plot of PPT data in far field of the pile.

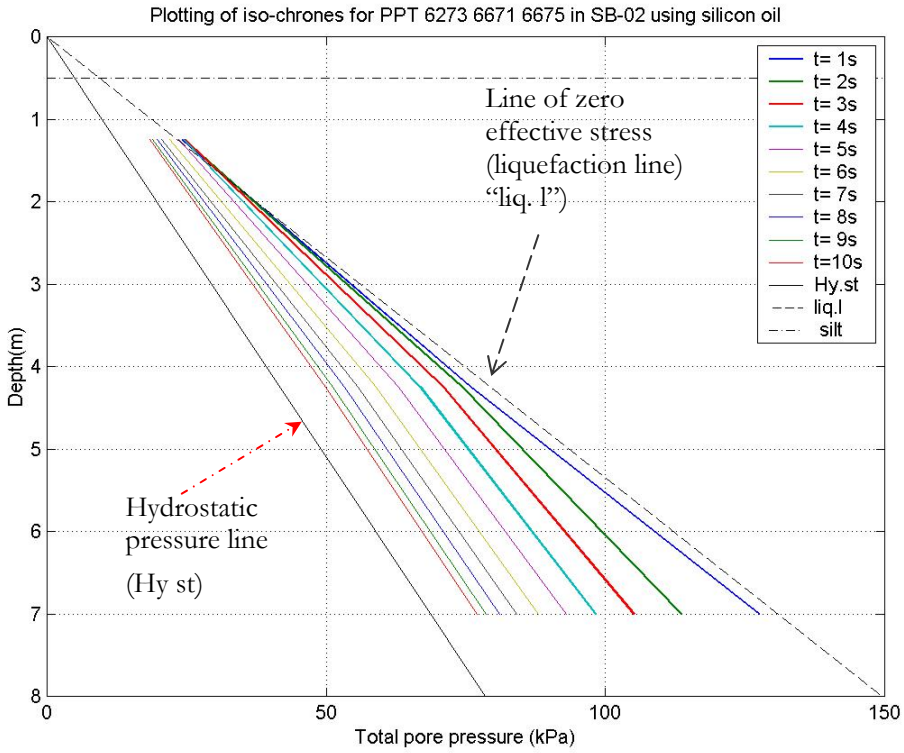

Figure 5.19: Plot of isochrones in test SB-02.

5.3.2 Buckling initiation

As mentioned earlier, test SB-06 was dedicated to understand some aspects of pile soil interaction during seismic liquefaction. A spring loaded LVDT was attached to pile 10 as shown in Figures 4.33 and 5.20, to identify the time of buckling initiation. Figure 5.20 also shows the instrumentation surrounding pile 10 with an estimate of the pre-existing effective vertical stress at the corresponding elevation.

Figure 5.21 plots the time histories of input acceleration, pore pressure records and the LVDT readings. It may be noted that as shaking starts pore pressures begin to rise but the pile starts to buckle after two full cycles of loading. This confirms that the buckling is not linked to inertia. It must also be observed from the plot that the pile begins to buckle before the bottom soil is fully liquefied (PPT 6266).

As discussed in section 5.3.1, a front of zero effective stress travels top-down during seismic liquefaction in a centrifuge test. It may be hypothesised that when this advancing front reaches a critical depth H_C given by equation 5.1 (Euler's formula), the pile would have become elastically unstable following equation 3.1, taking $L_{eff} = 2H_C$ for a pile with no restraint at the head.

$$H_c = \sqrt{\frac{\pi^2 EI}{4P}} \tag{5.1}$$

For pile 10, the critical depth is estimated to be 158mm from the point of application of the axial load, which is 18 mm below the level at which PPT 6675 was placed. Figure 5.21 shows that PPT 6675, which is 18 mm above H_C has liquefied, but PPT 6266 which is 32 mm below H_C has not liquefied fully, when the pile started to buckle. It may be concluded that PPT record verified the hypothesis of critical depth. This is further discussed in section 6.4.1

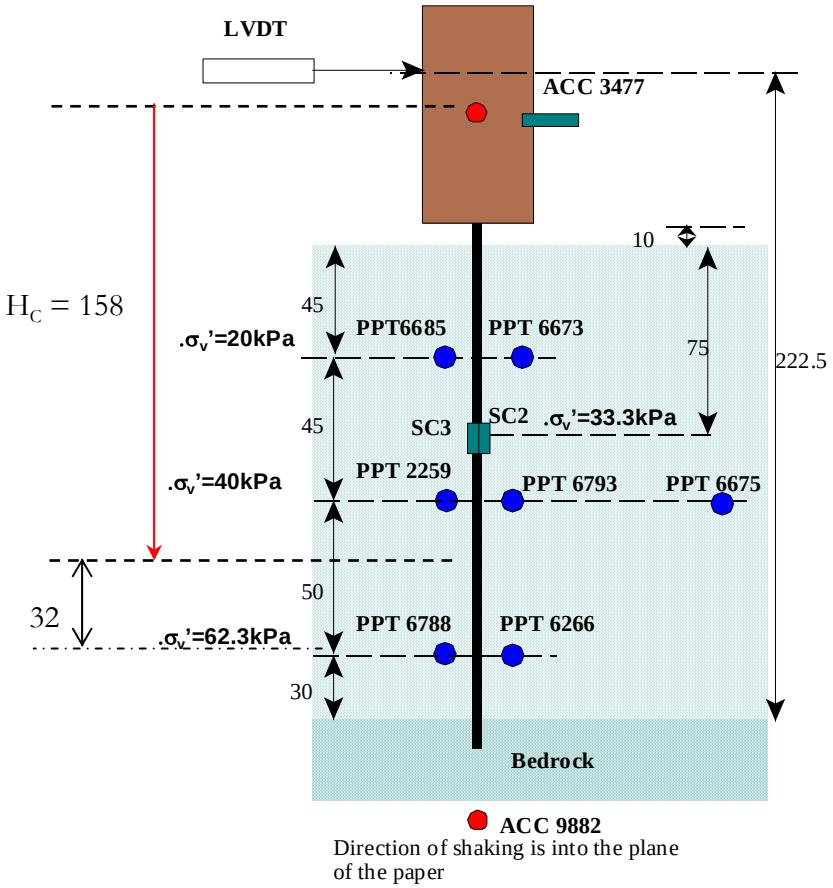

Figure 5.20: Instrumentation layout surrounding Pile 10 (all dimensions are in mm).

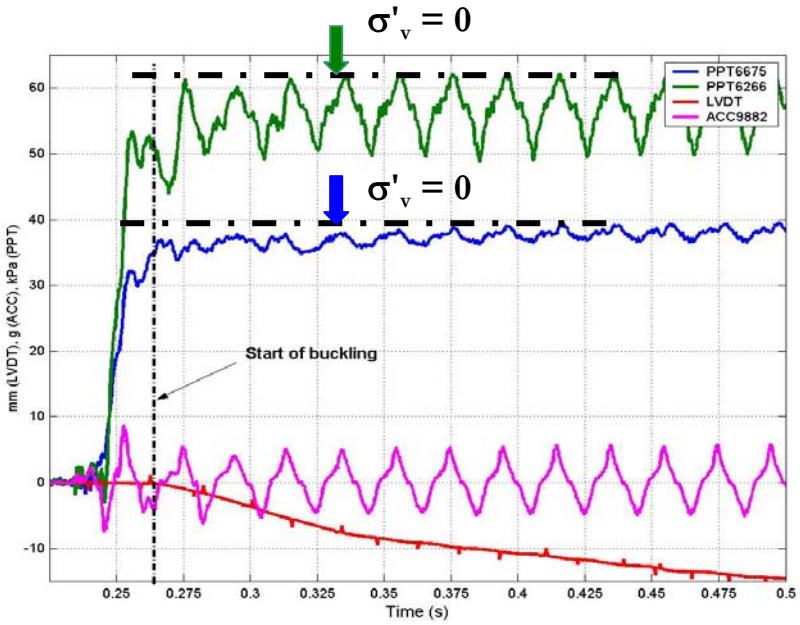

Figure 5.21: Time histories of input acceleration, pore pressure and LVDT reading for pile 10.

5.3.3 Near field pore pressures

With earthquake shaking, a front of zero effective stress advances top down and at the same time the length of the pile is gradually unsupported by the soil grains. The pile would begin to buckle sideways as the advancing front reaches the critical depth thereby pushing the soil. It must be expected that the imposition of monotonic shear strains (due to pile monotonically pushing the soil) at low effective stresses in moderately dense soil will lead to an attempt to dilate, suppressed by the need for water to flow into the zone affected, which must then create a local reduction of pore fluid pressure.

Figure 5.22 shows that the ultimate displacement δ of the top of the pile, when normalised by the pile diameter D, gives a reference shear strain (Goh and O'Rourke, 1999; Takahashi et al, 2002) of δ/D = 200%. This magnitude of shear strain is quite sufficient for the achievement of a Critical State in the shear zone. Figure 5.23 compares the PPT traces at shallow depth in the near field of the pile (PPT 6260 in front of the pile, i.e. in the direction of eventual buckling; PPT 6793 behind the pile) and the far field PPT J13.

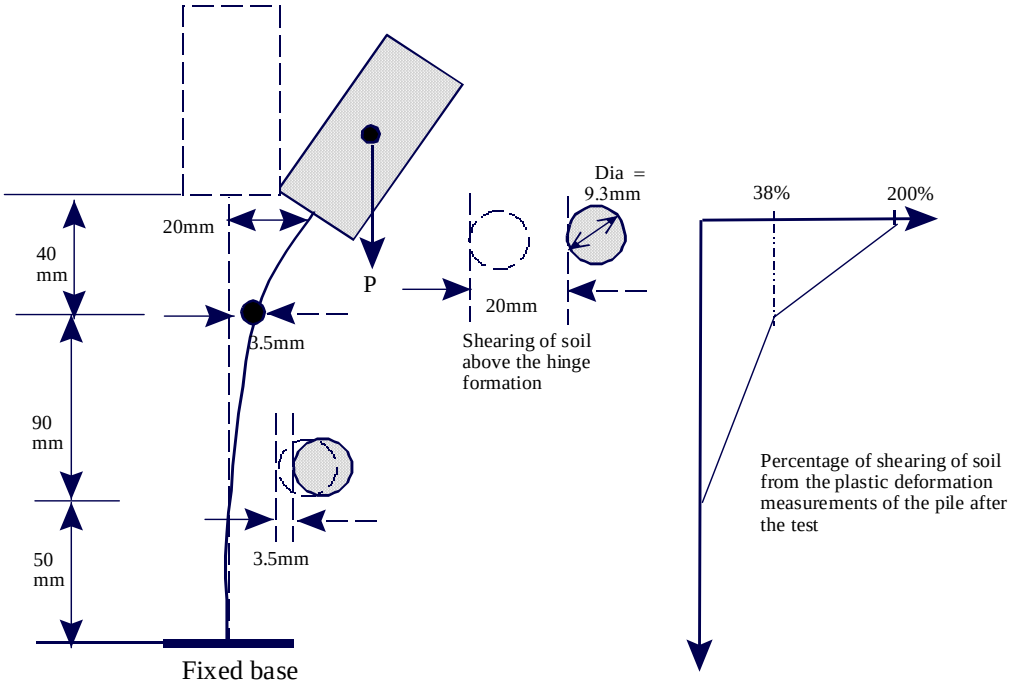

Figure 5.22: Plastic deformation measurements of pile 8 after test SB-04.

At first, up to 0.4 s, the three PPTs record the same pressures rising to the state of zero effective stress. Then, until 1.0 s the PPT in front of the pile (PPT 6260) shows a circa 10 kPa reduction of pore pressure with additional sharper downward spikes at each earthquake cycle. The PPT behind the pile (PPT 6793) shows positive spikes which are at first out of phase with those in front and which then come in phase. The cyclic component of the PPT data behaviour is clearly related to the shaking, and therefore to motions orthogonal to the eventual direction of buckling. But the steady component of pore pressure reduction in front of the pile must be due to suppressed dilation as the pile begins to push the previously "liquefied" soil aside. Evidently the soil in that zone is liquefied no longer, but enjoys a vertical effective stress of between 10 and 20 kPa – enough for the pile to receive significant support – again, temporarily.

By 1.0 s in the time record of Figure 5.23, however, the pore pressure reduction in front of the pile has diminished, due to transient inflow presumably, to the point where the positive spikes take the pore pressure in front of the pile back up to the "liquefaction" pressures of the far field. At that point the pile head load collapsed onto the surface of the saturated sand, when the pile plastically buckled. A tremendous *negative* spike of pore pressure is seen on PPT 6260 in front of the pile. This is attributed to the mass hitting the sand surface. By the time shaking ceases at 1.1 s this PPT is recording a steady 25 kPa pore pressure deficit compared with the "liquefied" far field, as the previously "liquefied" soil in the near field must now participate in the undrained

bearing capacity of the load, acting as a rather tilted shallow foundation. Because it must carry load, and because it can generate as much effective stress as it needs to achieve that, its pore pressure drops correspondingly.

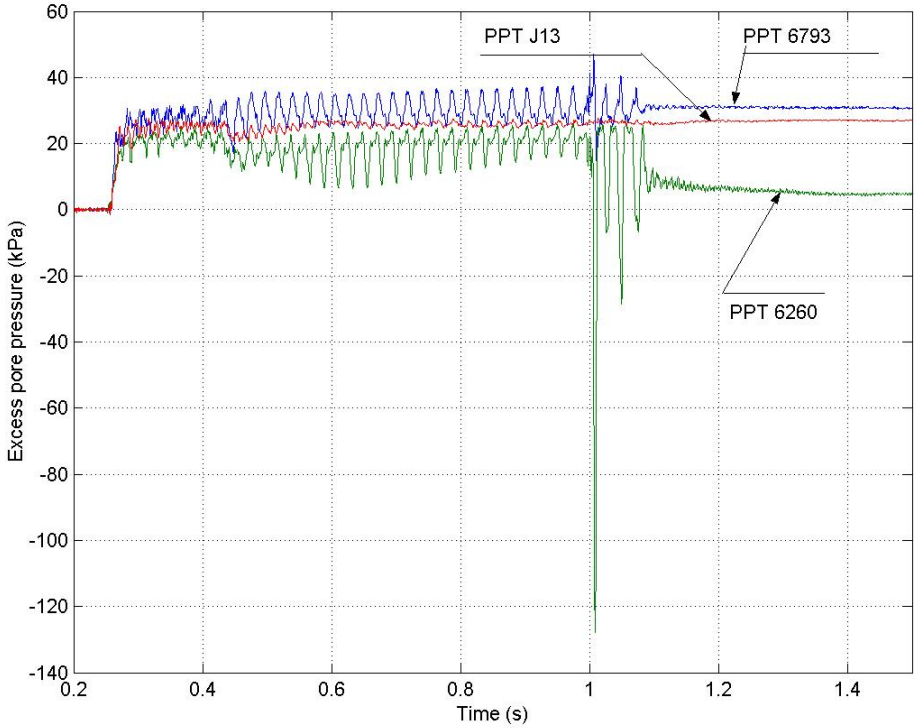

Figure 5.23: Near field (PPT 6260 & PPT 6793) and far field (PPT J13) pore pressure measurements at 52.5mm depth for pile 8.

Similar pore pressure records have been observed for pile 10 in test SB-06. Thus it is concluded that these observations are repeatable. A hypothesis of pile soil interaction is described in section 6.7.

5.3.4 Earth pressures on the front and back faces of the pile

Figure 5.20 shows the instrumentation layout surrounding pile 10 and Figure 5.24 shows photographs of the pile before and after the test. As mentioned earlier LVDT was placed at the top of the pile head to record the lateral movement. Earth pressure cells SC2 and SC3 were attached to the pile at 75mm depth (representing 3.75m depth of soil in the prototype scale) to record the pressure changes as the pile buckles. The estimated effective stress at this level is 33.3kPa, (see Figure 5.20).

(a) (b) (c)

Figure 5.24: Pile 10 in test SB-06; (a): Stress cells attached to the pile; (b): The pile during excavation; (c): Deformed shape after the excavation.

Pile 10 was subjected to axial load alone and from Figure 5.24 it must be noted that two hinges were formed. As mentioned in Table 5.1, in test SB-06 due to some mechanical problems the actuator fired a second earthquake; the input motion is shown in Figure 5.25. It is evident from the LVDT reading (Figure 5.26) that the pile failed during the first earthquake. It is possible that the bottom hinge may be due to the second earthquake when the pile head mass acted as an inclined footing and imposed lateral force on the pile.

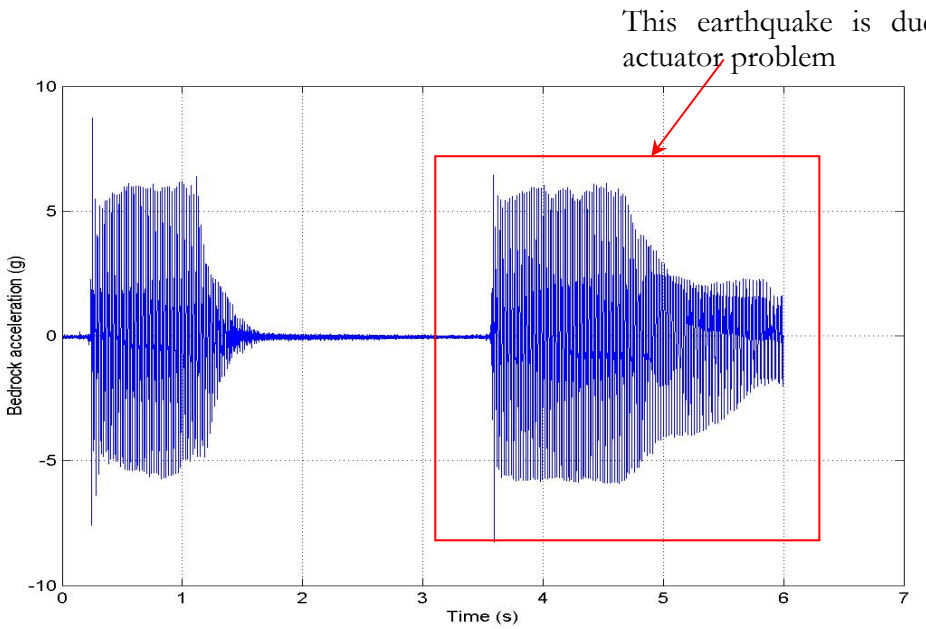

Figure 5.25: Input motion in test SB-06

From the time history of LVDT reading (Figure 5.26) it can be noted that the gradient of the displacement decreases with the progression of pile movement i.e. buckling. In other words, the pile is having negative acceleration or deceleration and the opposing force must be the resistance of the liquefied soil. In the plot, three parameters are shown in a text box, the values of which correspond to the level of the pressure cells i.e. at 75mm depth. The parameters are:

1. **Velocity of buckling** (V): It is the rate at which the moving pile loads the soil and it can be linked to the shear strain rate of the neighbouring soil.
2. **Normalised displacement of the pile** (δ/D): δ is the pile displacement and D is the diameter of the pile. It is proportional to the shear strain of the soil. As mentioned earlier, this parameter has been used by Goh and O'Rourke (1999), Takahashi et al. (2002) Haigh (2002).
3. **Normalised velocity of buckling** (V/k) where k is the permeability of the soil. This parameter can describe the type of loading, for example drained or undrained. This parameter has been used by Takahashi et al (2002) to study the lateral resistance of piles in liquefied soil.

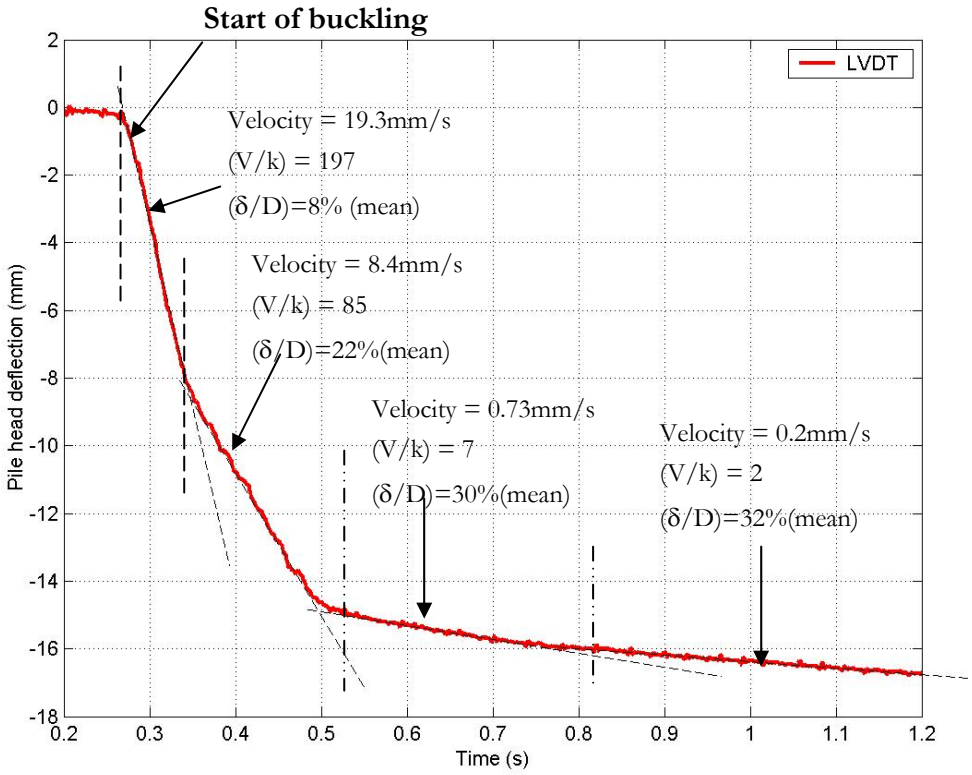

Figure 5.26: Displacement record of the LVDT

The pile displacement (δ) at the level of the earth pressure cells is estimated from the LVDT record using a parabolic mode shape ($y = A.x^2$) where A is a function of applied moment. This is essentially the deflection expression of a cantilever beam with moment (M) applied at the free end. It can be justified by the fact that the moment due to the "out of line axial force" is causing the curvature in the pile. Accounting for the soil stiffness will also give a mode shape of second order, but a complicated function of exponential and harmonic, Hetenyi (1946), and is not attempted here. However as the deflection is scaled down proportionally the error would be very marginal.

Figure 5.26 shows that the pile initially moved by 8mm without much lateral resistance and then as shearing continues the lateral resistance increases and as a result velocity of pile decreases. Other researchers, Towahata et al. (1999), Takahashi et al (2002), have reached similar conclusions that initial resistance to movement is negligible but some lateral resistance is mobilised after a certain amount of displacement. This is further discussed in section 6.6.

Figure 5.27 plots the time history of the pressure readings recorded by the pressure cells. It may be noted from the figure that the pressure cells SC2 and SC3 recorded a difference of 16kPa

before the earthquake, which should ideally be zero. This can be attributed to the fact that at 50-g during the release of the piston, shown schematically in Figure 4.32, and before the occurrence of earthquake, the pile head moved when it was freed from the support. This is the tolerance of the experimental set up consisting of the special frame described in section 4.10.1. The movement of the pile was recorded by the LVDT during the swing up. At the level of stress cells this movement is estimated to be 0.6 mm and may have mobilised some passive resistance.

The difference in the stress cell readings approximately measures the lateral resistance offered by the liquefied soil to the buckling pile. The lateral resistance measured is normalised by the initial over burden pressure (33kPa) at the level of the pressure cells. Figure 5.28 shows the plot of normalised lateral resistance with the normalised displacement of the pile (δ/D). It may be noted that lateral resistance increases drastically after 30% of reference strain, which also substantiates the LVDT record (see Figure 5.26).

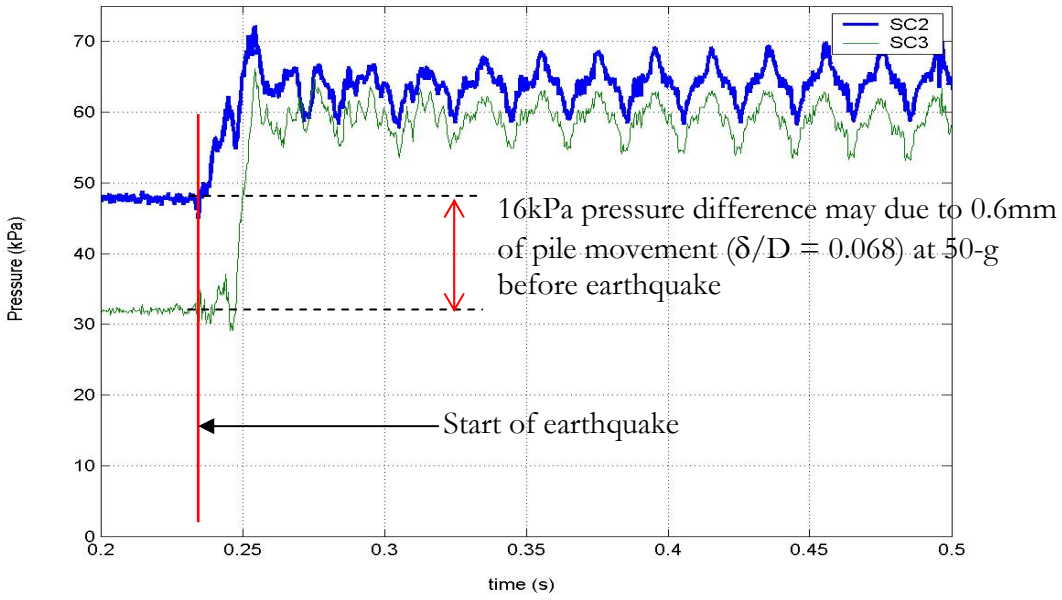

Figure 5.27: Pressure cell readings in test SB-06.

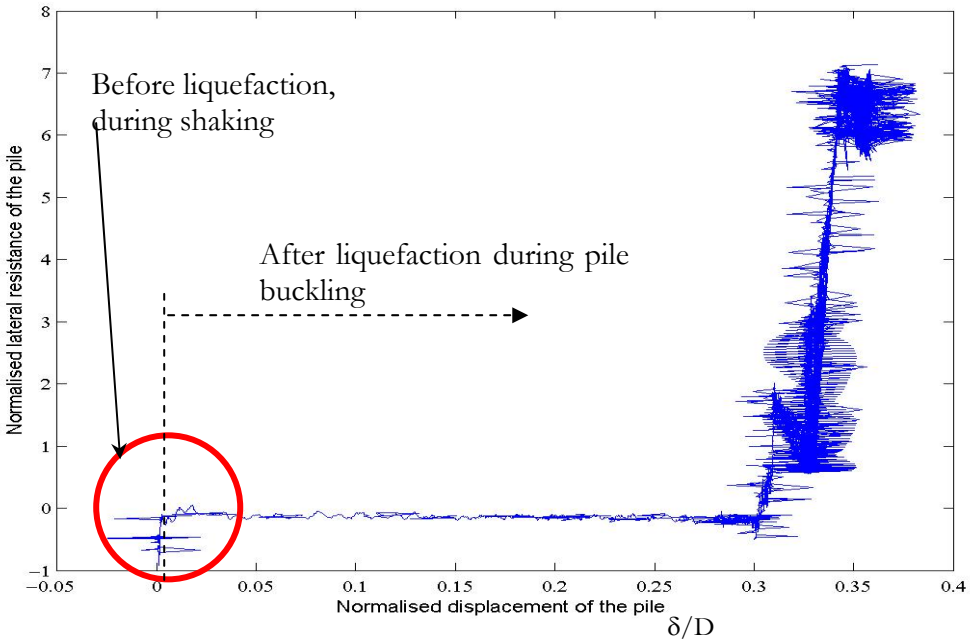

Figure 5.28: Normalised lateral resistance versus normalised lateral displacement.

Figure 5.29 plots the time histories of difference in stress cell readings, LVDT, PPT's and input acceleration for the first 0.5seconds, which corresponds to the lateral movement of the pile for the first 15mm. Initially, as shaking starts the pressure difference across the pile increases until the point where the soil most likely fails due to excessive shear straining due to the earthquake. At this point the pore pressure is nearly hydrostatic and the pile is stable, thus supporting the argument that the drop of pressure change takes place due to soil failure. In the next half cycle pore pressures rise starting from the top and proceeding towards the bottom. The pile starts to buckle as seen from a sharp change in pressure difference. As the pile buckles, pushing the initially liquefied soil, the resistance remains fairly constant till the time instant of about 0.4sec, after which resistance increases. Figure 5.30 tracks the pressure changes during the movement of the pile in order to identify the different mechanisms.

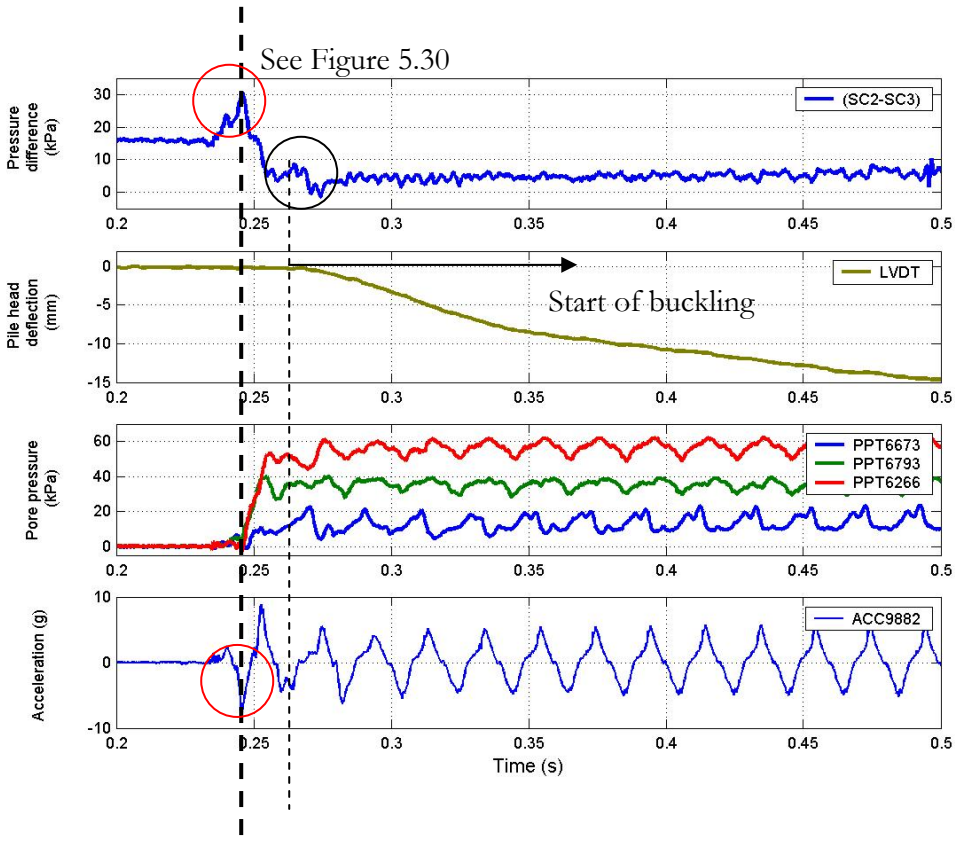

Figure 5.29: Time history of LVDT, PPT's input acceleration and pressure cells.

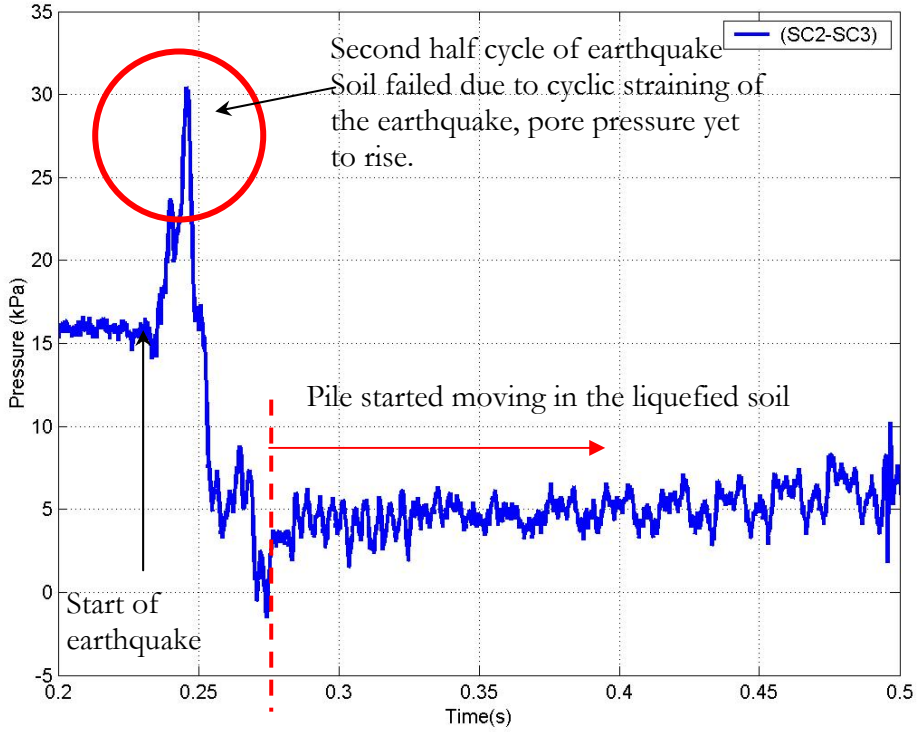

Figure 5.30: Time history of the difference in pressure cell readings.

5.4 Behaviour of pile under the combined action of axial load and inertia

Following Figure 5.12 it may be noted that the behaviour of piles under combined axial and bending stresses can be classified into two groups. They are

1. The piles that failed during earthquakes.
2. The piles that did not collapse during earthquakes and remained in stable equilibrium.

This section of the chapter discusses the behaviour of these piles as observed in the centrifuge tests.

5.4.1 Failure of pile under combined bending and axial load

It is well known that, imperfections such as, lateral loads or out-of-line straightness increases lateral deflections, which in turn induces plasticity in the strut and reduces the buckling load, promoting more rapid collapse. This would imply that in presence of lateral load, an unsupported pile would buckle at a load lower that P_{cr}. It will be seen later (section 6.4, Figure 6.2) that for unsupported columns having (P/P_{cr}) ratio of about 0.65 the deflection due to lateral load amplifies by three times due to the P-δ effect (Figure 6.2).

Pile 12 in test SB-06 had a P/P_{cr} ratio of 0.75 and failed during the earthquake under the combined action of inertia and axial load. Figure 5.31(a) shows the instrument layout surrounding pile 12. This figure also shows a schematic shape of the pile at failure, which can be compared with the actual deformed shape shown in Figure 5.31(b). This shape suggests that the resistance of the liquefied soil is enough to stop the development of full height buckle. A simple experiment is carried out to demonstrate the bi-linear nature of the buckled pile and is described in section 6.8. Similar behaviour is witnessed in Pile 3 in test SB-02.

Figure 5.32 plots the time history of pore pressure, input acceleration and the acceleration transmitted to the pile head mass. It may be noted that Pile 12 started to buckle when the entire soil liquefied. The horizontal inertia force exerted on the pile head mass during the initial shaking period is $2\times9.8m/s^2\times0.9kg = 17.6N$. A detailed analysis of bending and buckling using "Beam-columns on elastic foundation", Hetenyi (1946) taking into account the stiffness degradation of the soil is carried out later in section 6.9.1.

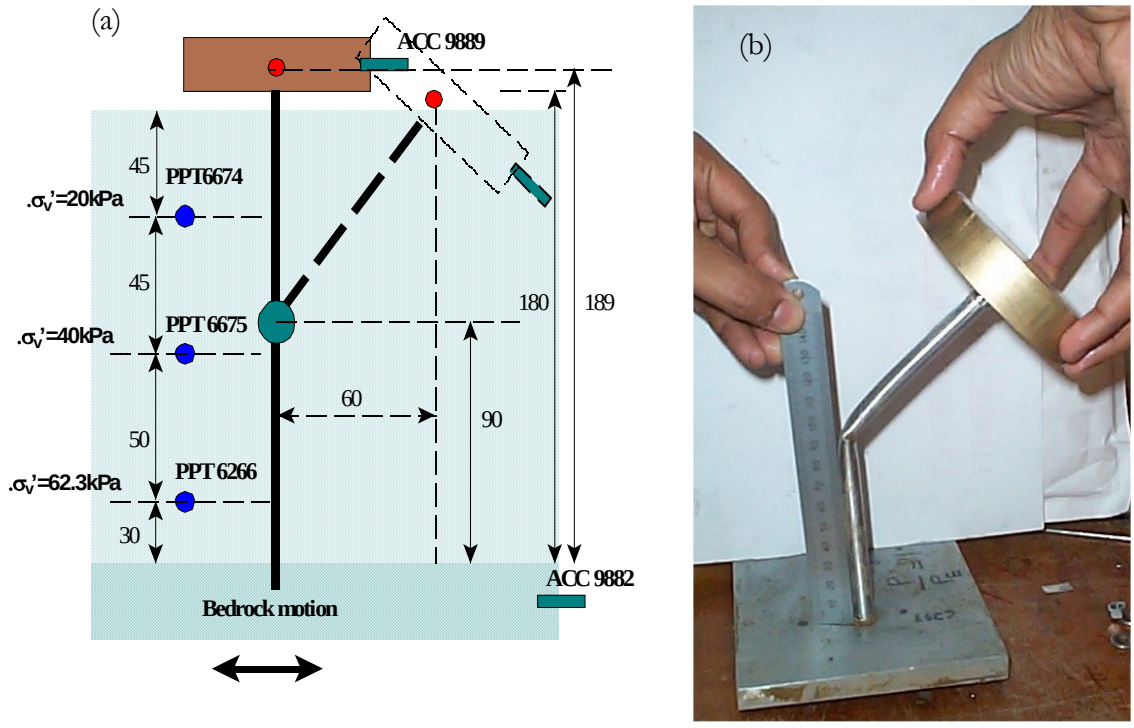

Figure 5.31: Pile 12; (a): Instrument layout surrounding the pile; (b) Final deformed shape.

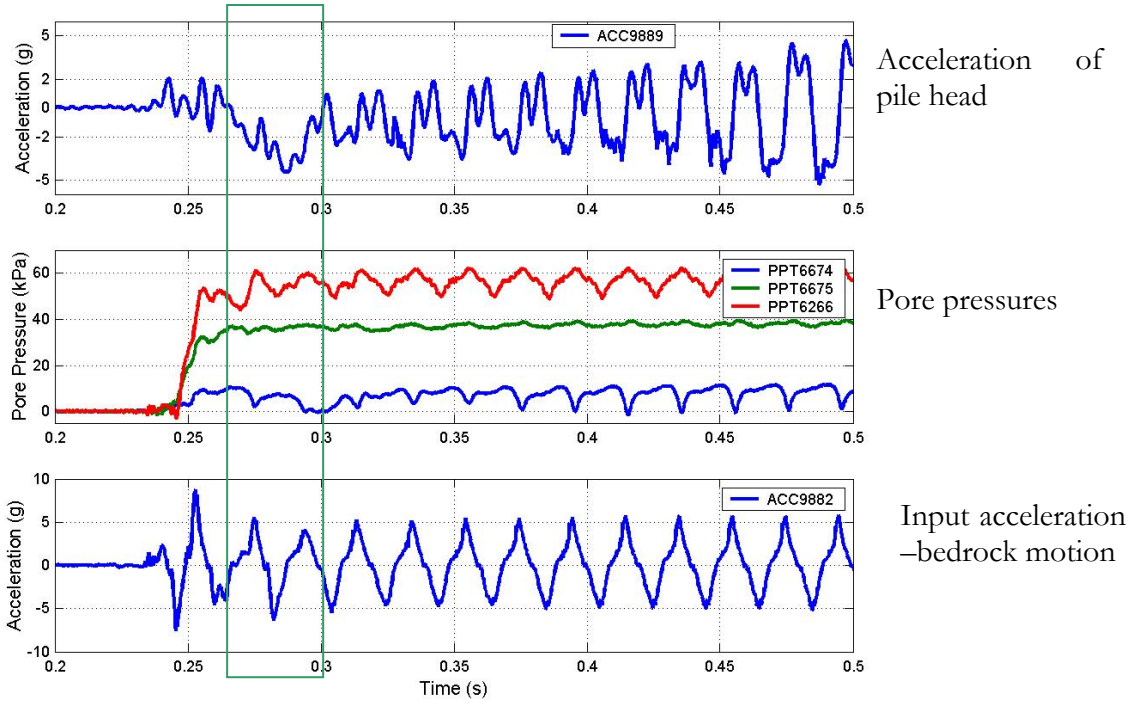

Figure 5.32: Time history of input acceleration, pore pressures and acceleration of the pile head for pile 12, the instrumentation layout is shown in Figure 5.31(a).

The acceleration time record in Figure 5.32 may be interpreted as follows. At an instant of about 0.26sec the entire length of the pile would have been unsupported by the soil grains and the pile became unstable under the combined action of lateral inertial load and axial load. The pile buckles sideways under the increased P-δ moment and eventually the pile head touches the ground, (see Figure 5.33). The resistance to the motion of the pile is due to the liquefied soil in front of the pile as well as due to the pile head acting as an inclined footing. Of particular interest is the penetration of half of the circular brass plate in the liquefied soil. The penetration is measured to be approximately 42mm i.e. 2.1m in prototype scale. This is not surprising in field scale as can be seen in Figure 1.1(c) where an entire raft overturned.

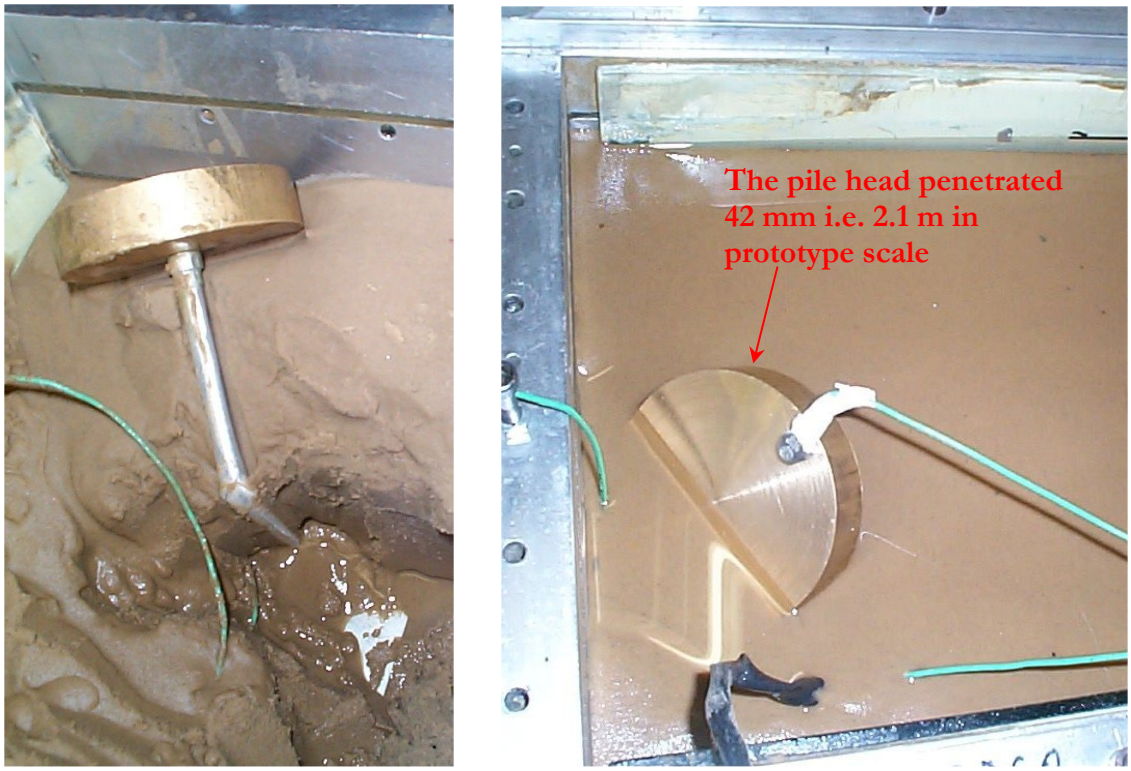

Figure 5.33: Failure of pile 12 during earthquake in test SB-06

5.4.2 Piles that vibrated and did not fail during seismic liquefaction

As schematically shown in Figure 5.12, piles having P/P_{cr} ratio below 0.5 did not fail under the combined action of inertia and axial load. In each of these cases multiple earthquakes took place. This is consistent with the study of case histories where piles having P/P_{cr} between 0.5 and 1.0 failed irrespective of the type of ground (i.e. level or sloping) and piles having P/P_{cr} below 0.1 did not fail. This is further discussed in section 6.4.

Figure 5.34 shows the accelerometer locations for pile 11 in test SB-06. It must be noted that the accelerometers were placed to measure the transfer of input acceleration to the pile head as soil liquefies due to the stiffness degradation of the pile-soil system. Figure 5.35 plots the input acceleration and the acceleration transmitted to the pile head. From the acceleration record it is observed that the motion of the pile is initially in phase, i.e. in the first half cycle before soil starts to liquefy and during shaking. With the progression of pore pressure rise in a top-down fashion, the stiffness of the pile-soil system decreases and the motion of the pile is out of phase. After full liquefaction i.e. just after the instant of 0.3 sec in the time record the motion of the pile comes in phase with the input acceleration.

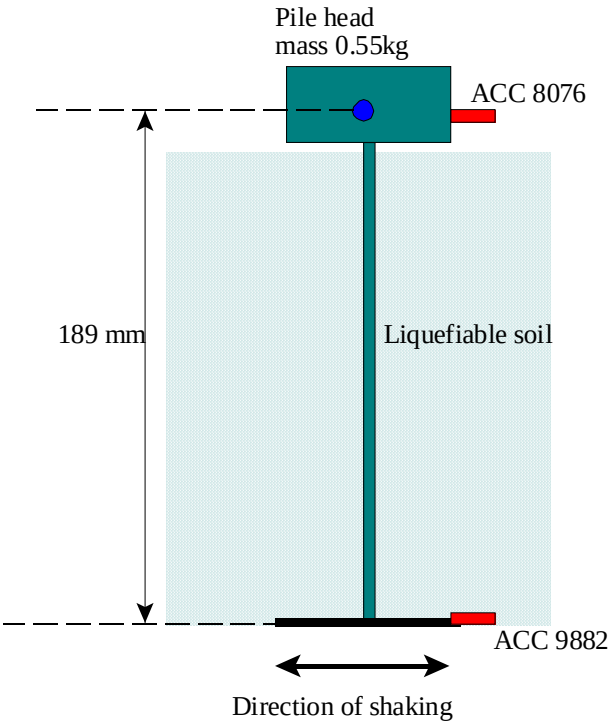

Figure 5.34: Accelerometer locations for pile 11.

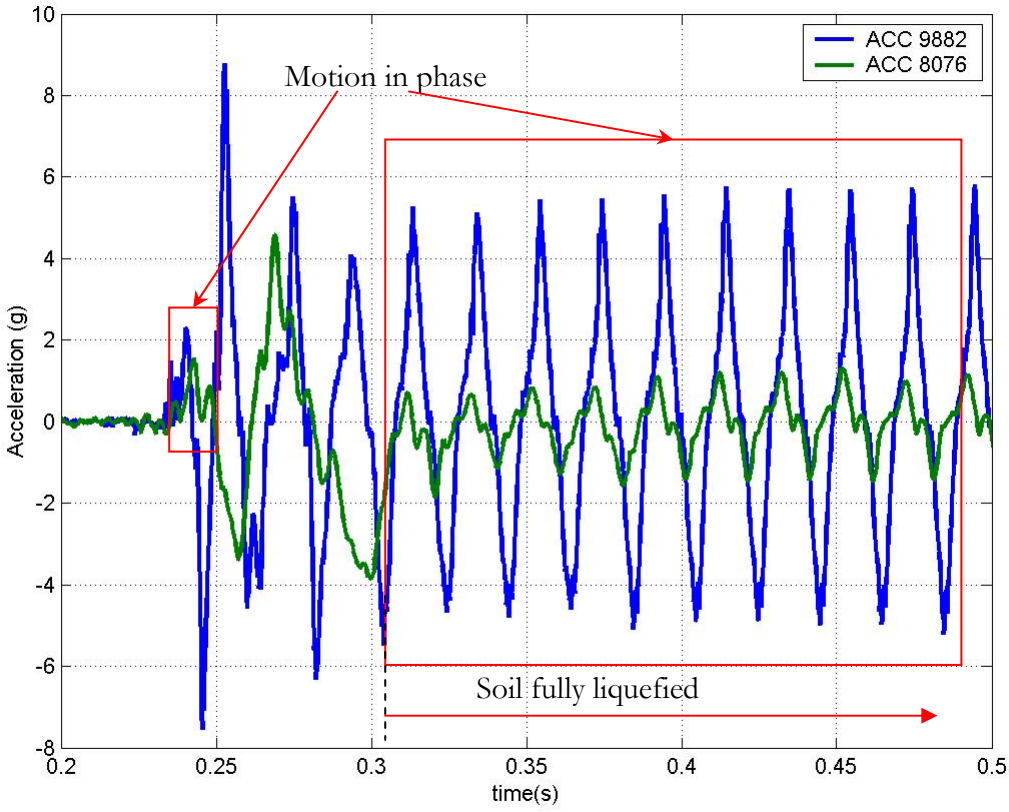

Figure5.35: Acceleration record of pile mass and the input acceleration

The motion of the pile-soil system as shown in Figure 5.34, in absence of soil, can be modelled well as a Single Degree of Freedom (SDOF) system. However, when the effect of soil needs to be included in analysis, the system becomes complex. In the present study an attempt has been made to draw some analytical observations based on a simplified SDOF system assumption having equivalent soil-pile stiffness, damping and mass.

The standard equation of motion for a harmonically excited SDOF system can be represented by equation 5.2, Clough and Penzien (1993)

$$M\ddot{x} + C\dot{x} + K_{ps}x = F_0 \sin(\omega t) \qquad (5.2)$$ where

x = Displacement of the system and (.) represents the first derivative with respect to time.

M = Mass of the pile soil system

C = Damping

K_{ps} = Stiffness of the pile-soil system

F_0 = Amplitude of the forcing function

ω = Frequency of the forcing function, which is predominantly 50Hz in this case.

In dynamics problems, the standard Dynamic Amplification Factor (D.A.F) for a SDOF is estimated following equation 5.3

$$D.A.F = \frac{X}{\left(\frac{F_0}{K_{ps}}\right)} = \frac{1}{\sqrt{\left[1-\left(\frac{\omega}{\omega_n}\right)^2\right]^2 + \left[2\rho\left(\frac{\omega}{\omega_n}\right)\right]^2}} \qquad (5.3)$$ where

X = Amplitude of displacement during the dynamic event

ρ = Damping ratio

ω_n = Natural frequency of the system under undamped oscillations.

Figure 5.36 plots equation 5.3 for different damping ratios. The DAF is estimated for the pile-soil system (Figure 5.34) by taking ratios of the magnitude of input acceleration and the transmitted acceleration as in Figure 5.35. Table 5.3 tabulates the DAF for few cycles. As shown in Table 5.3, for the first half cycle of earthquake, when the soil is yet to liquefy, the DAF = 0.65 which gives ω/ω_n = 1.6 following Figure 5.36. The frequency of the pile-soil system is thus estimated as 31Hz. Subsequently, DAF gradually reduces and hence the frequency of the pile-soil system reduces. This confirms the well-known fact about continuous degradation of soil stiffness due to liquefaction. This is shown by the green arrow in Figure 5.36.

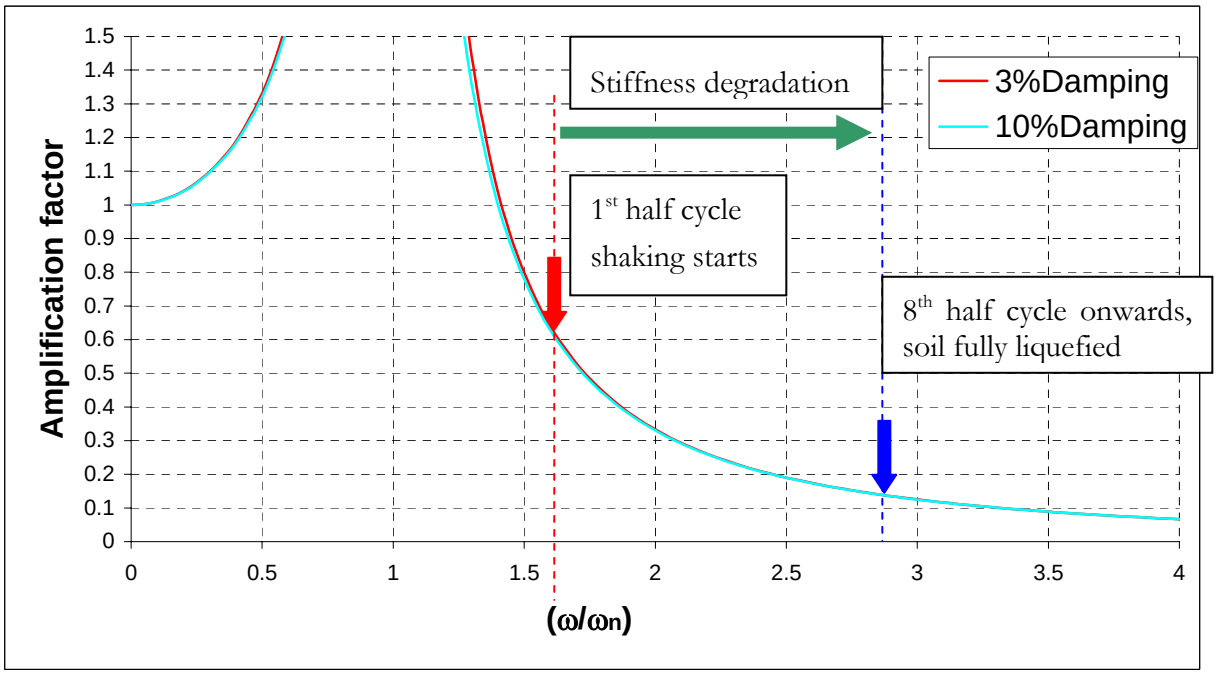

Figure 5.36: Dynamic amplification factor for a SDOF system.

Table 5.3: Dynamic Amplification Factor observed in pile 11.

Cycle of earthquake	D.A.F (from Figure 5.35)	ω/ω_n (from graph 5.36)	Frequency of pile-soil system
1st Half-cycle	0.65	1.6	31Hz
2nd Half-cycle	0.43	1.75	29Hz
8th Half-cycle and onwards	0.17	2.8	18Hz

* ω = forcing frequency = 50Hz

The frequency of a fixed base pile in absence of soil is estimated using equation 5.4.

$$\omega_n = \frac{1}{2\pi}\sqrt{\frac{3EI}{ML^3}} = 13\text{Hz} \qquad (5.4)$$ where

EI = Stiffness of the pile = 7.77×10^6 Nmm^2 (see Table 4.11)

L = length of the pile = 189 mm, Figure 5.34

M = 0.55kg

The results of the above simple analysis may be interpreted as follows:

- Initially before liquefaction and during shaking, the pile-soil system acted as a coupled system. This can be justified by the fact that DAF is 0.65, which is very high when compared to the DAF expected if pile would have acted alone, which is approximately 0.1.
- Once the surrounding soil liquefies the frequency of the pile-soil system (18Hz) comes close to the frequency of the pile in absence of the soil i.e. 13Hz.

5.5 Summary

A series of five centrifuge tests have been carried out to investigate the effect of axial load on a piled foundation as the surrounding soil liquefies in an earthquake. It has been shown that in a liquefiable layer, soil liquefaction starts from top and progresses downwards. At the same time soil grains surrounding a pile loses contact with the pile and the pile experiences a loss of confining pressure. As this advancing liquefaction front reaches a critical depth a pile would become elastically unstable and starts to buckle in the direction of least elastic bending stiffness. The initial resistance of the liquefied soil to the buckling pile would be minimal but some lateral resistance would act after a certain amount of displacement of the pile. The buckling of pile is in some way different from Euler's classical buckling theory. The pile buckling can be described as "*Euler's classical buckling of slender columns in a non-linear resistive medium*".